Okinawa Institute of Science and Technology

Graduate University

Thesis submitted for the degree

Doctorate of Philosophy

Nature and source of animal spontaneous behaviors: Insights from psychobehavioral development and neuronal population dynamics in mice

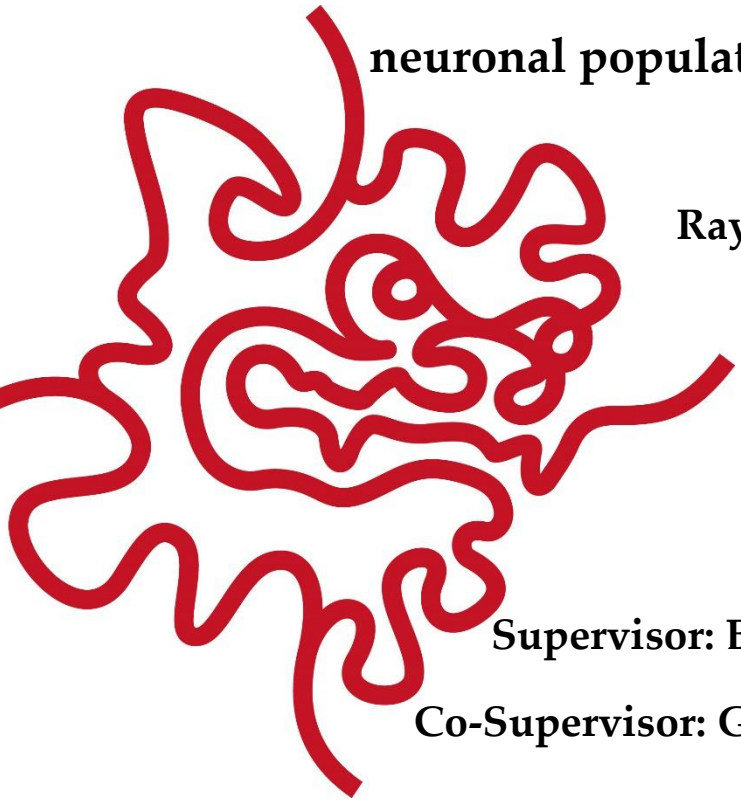

by

Ray Xin Lee

Supervisor: Bernd Kuhn, Ph.D.

Co-Supervisor: Greg J. Stephens, Ph.D.

July 23rd, 2018 (v1); November 15th, 2018 (v2)

Declaration of Original and Sole Authorship

I, Ray Xin Lee, declare that this thesis entitled "Nature and source of animal spontaneous behaviors: Insights from psychobehavioral development and neuronal population dynamics in mice" and the data presented in it are original and my own work.

I confirm that:

- No part of this work has previously been submitted for a degree at this or any other university.
- References to the work of others have been clearly acknowledged. Quotations from the work of others have been clearly indicated, and attributed to them.
- In cases where others have contributed to part of this work, such contribution has been clearly acknowledged and distinguished from my own work.
- None of this work has been previously published elsewhere, with the exception of the following: (*Corresponding author)

  Affective bonding explains post-traumatic behavioral development in adult mice.
  Lee R. X.*, Stephens G. J., & Kuhn B.
  eLife (under revision) [***bioRxiv***, 249870. January 18th, 2018 | doi: 10.1101/249870]

Signature: 

Date: July 23rd, 2018

Nature and source of animal spontaneous behaviors:
Insights from psychobehavioral development and neuronal population dynamics in mice

by
Ray Xin Lee

Submitted to the Graduate School in partial fulfillment of the requirements for the degree of Doctorate of Philosophy at the Okinawa Institute of Science and Technology Graduate University

Abstract

Awake animals switch between different behavioral states irregularly even in a homogenous and steady environment, especially obvious outside from any behavioral task when they are free to voluntarily behave. These irregular but structured patterns have been taken as a representation of internal states such as emotion, and are believed to represent underlying background brain activity and its dynamics. To date, the nature and source of animal spontaneous behaviors remain as a major conceptual challenge to academia, due to the lack of approaches to systematically and quantitatively examine this fundamental process. To achieve insights about the neural substrate of animal spontaneous behaviors, the research was conducted in two directions: (i) To interpret previously challenging and inconclusive behavioral development by re-evaluating spontaneous behaviors that represent emotionality, centered on the study of PTSD (post-traumatic stress disorder)-like internal psychological development in laboratory mice; (ii) To demonstrate a driving and control principle explaining fine-scale and global observations of neuronal and behavioral dynamics in spontaneously behaving mice, by two-photon calcium imaging of neuronal populations across cerebral cortical layers and areas. The results from these investigations provide the first system-level view of experimentally disentangled components, processes, and determinants explaining the nature and source of animal spontaneous behaviors.

Table of Contents

List of Figures

1 General Introduction

1.1 Ontology of volition and consciousness in scientific perspectives

"Sometimes when we act, it is in our power not to act; and sometimes when we do not act, it is in our power to act. In sort, it is sometimes within our power to act other than we do." (Cornman et al 1992) As a conceptual matter following this intuitive argument, volitional behaviors are actions hypothesized by libertarians to begin with a basic mental action (i.e. volition) which is required for an action to be left open by physical causation, as a free-willing behavior (Clarke 2002). Animals in nature show an impressive capability to choose a course of action from among various alternatives and are therefore believed to produce volitional behaviors. To probe into the reasoning that leads to this belief, it could be considered as an anthropomorphizing conclusion from the intuitive argument which makes an analog between a subject's own experiences and the animals observed by him/her (Nagel 1974). The subject's own experiences discussed here are the first-person experiences about the intention when s/he consciously initiates an action (Brembs 2010). The scope of these self-initiated behaviors ranges from tightly planned actions with high flexibility (e.g. context-dependent decision making) to loosely planned actions with high uncertainty (e.g. spontaneous behaviors arisen in a homogeneous environment). To examine and question the hypothesized non-physical components of volition and consciousness in the free will debate leads toward a previously mysterious research domain in science, and undoubtedly with a close relation to neuroscience.

Starting from the essential properties of phenomenal experience, a potentially proper understanding of the relationship between consciousness and the brain, such as the integrated information theory (IIT), has begun to be established (Tononi 2004). Instead of starting from matter and "squeeze" consciousness out of it, IIT starts from consciousness itself and ask what physical system could account for its properties. This approach is similar to the derivation of a conceptual and mathematical

framework for evaluating the quality and quantity of "temperature" or "color" in physics. The IIT axioms of essential properties of experience are intrinsic existence (consciousness exists), composition (consciousness is structured), information (consciousness is specific), integration (consciousness is unified), and exclusion (consciousness is definite). Correspondingly, their associated postulates of the required properties of the physical substrate of experience, as the inferences that go from phenomenology to physics, are the cause-effect power with respect to "intrinsic existence", the power-set structure with respect to "composition", the differentiated repertoires with respect to "information", the intrinsic irreducibility specified by unidirectional partitions with respect to "integration", and the definite grain size in space and time with respect to "exclusion". Accordingly, together with the quantitative measure of intrinsic irreducibility as the integrated information, IIT argues that "the physical substrate of consciousness is a maximum of intrinsic cause-effect power" (Oizumi et al 2014), a form in cause-effect space. IIT for the physical substrate of consciousness has been validated by its strong explanatory and predictive power, precisely and scientifically, to previously inaccessible questions, such as "Why does the cortex support consciousness when the cerebellum does not, despite having four times as many neurons?", "Why does consciousness fade during deep sleep while the cerebral cortex remains active?" (Tononi et al 2016), "Are animals that display complex behaviors, but have brains very different from humans, conscious?" (Boly et al 2013) Following the postulates which request that a conscious system should be a system with intrinsically causal structures, an understanding of the associations between internal and external causal interactions is therefore critical to fully explain the distributed spatiotemporal patterns arisen spontaneously. This issue emphasizes the necessity to scientifically address the nature and source of animal spontaneous behaviors by matching between internal and external cause-effect structures, for a complete understanding of how a single system can flexibly be free from external causes and determined by internal causes, and *vice versa*, to achieve its adaptation in the complex and uncertain environment.

Unlike the theoretical advances toward the physical substrate of consciousness, hypotheses explaining animal spontaneous behaviors remained vague and not mutually exclusive. In human studies, although it has remained highly controversial (Banks & Isham 2009, Haggard 2008, Haggard & Eimer 1999, Lau et al 2004, Lau et al 2007, Libet 2003, Trevena & Miller 2010, Velmans 2003), the first awareness of the wish or intention reported by subjects has been suggested to be preceded by the brain activation for a freely voluntary act (Fried et al 2011, Kühn & Brass 2009, Libet et al 1983, Matsuhashi & Hallett 2008). Furthermore, prediction of decision activity was reported to be achieved from referring the spontaneous activity 0.5 s or more before the decision cues are provided, as a computational approach in testing free will (Rolls & Deco 2011). These results indicated an intrinsically deterministic mechanism for voluntary acts in general. Extending the time scale, spontaneous behavioral dynamics in a large number of species show complex features of irregular alternation between different states [e.g. fruit flies (Maye et al 2007, Reynolds & Frye 2007), mice (Nakamura et al 2008, Proekt et al 2012), rats (Kafetzopoulos et al 1997, Yadav et al 2010), spider monkeys (Ramos-Fernández et al 2004), and humans (Brockmann et al 2006, Nakamura et al 2007, Nakamura et al 2008, Song et al 2010)]. Diverse body shapes of spontaneously behaving nematodes (*Caenorhabditis elegans*) were further reported to display in a low dimensional space (Stephens et al 2011a, Stephens et al 2008, Stephens et al 2011b), with brain-wide neuronal dynamics embedded in a low-dimensional attractor-like manifold of the neuronal activity space (Kato et al 2015). These discoveries imply that temporal organization of animal spontaneous behaviors might highly depend on internal causes and be highly independent to external causes, such as the intermittency of an itinerant associative dynamic produced by a simplified model (Dunn et al 2016). Ambivalently, brain activity has been known to be strongly and widely affected by external inputs from both environments and animals' own behaviors (Stringer et al 2018). While numerous computational processes of sensory feedbacks from self-generated movements (reafference) are required for proper behaviors (Angelaki & Cullen 2008, Cullen 2011, Rochefort et al 2013), these

observations and investigations point out the issue of the controlling processes beyond self-organizing dynamics to explain animal spontaneous behaviors (Lee et al 2015). To date, the fundamental control mechanisms and dynamic processes associating externally expressed behavioral reactions and internally organized neuronal activities for spontaneous behaviors remain elusive.

1.2 Animal internal states represented in behaviors

''Certain states of the mind lead […] to certain habitual movements.'' "[T]he internal consciousness that the power or capacity of the nervous system is limited, will have strengthened […] the tendency to violent action under extreme suffering." "Even insects express anger, terror, jealousy and love, by their stridulation." (Darwin 1872) While basing on romantic anthropomorphizing from personal intuition, in the sense of lacking consistent and operational criteria, the statements reflect a long-standing belief that emotion should be represented in behaviors that are shown. For pet dogs, similarly, they were demonstrated to be able to discriminate between emotional expressions of heterospecifics beyond responding according to simple cues (Müller et al 2015). These ideas bring a possibility for relatively simple approaches to demonstrate emotion (e.g. as a first-person experience) by qualitatively and quantitatively measure its observable components (i.e. emotionality) of emotional representation.

In fact, animal spontaneous behaviors in a designed environment or their reaction in a designed experimental task has been taken as a read-out of their internal states such as emotion (Archer 1973). Holding the aim to generalize and standardize the concept of emotion in scientific studies, a recent review argued that "emotion states exhibit certain general functional and adaptive properties that apply across any specific human emotions like fear or anger, as well as across phylogeny", proposing four emotion primitives: the scalability (intensity of emotion), valence (opposite emotion states), persistence (outlast the stimuli that elicit them), and generalization (influence subsequent responses to different stimuli) (Anderson & Adolphs 2014).

While centering around experimental data and potential applications, the arguments, however, poorly provide a structural reasoning to support the necessity and sufficiency of proposed criteria as a theoretical foundation, by showing how competitive views are misleading and how the proposed view with advanced novelties is more reasonable, instead of stated in a way to presume and mainly focus on their technical advances. Therefore, scientific studies toward psychobehavioral, psychodevelopmental, and psychopathological mechanisms has been largely limited by the lack of an empirical study complemented by a solid theoretical approach.

1.3 Concluding remarks

Based on the foregoing, the aim of my research is to develop novel approaches to interpret previously challenging psychopathological development by using laboratory mice and address previously inaccessible research problems about the association between spontaneous behavioral and cortical neuronal dynamics in laboratory mice.

2 Uncover PTSD-like internal psychological development

2.1 Introduction

Post-traumatic stress disorder (PTSD) is one of the most prevalent mental health disorders and has received serious clinical and research attention (DSM-5 2013, DSM-III 1980). Still, it remains as one of the most poorly understood and controversial presentations of psychiatric disorders (McFarlane 2010). The debates have even questioned the existent of PTSD (McHugh & Treisman 2007, Walton et al 2017), centered on its diversity, inconsistency, and delayed onset of symptoms even after a protracted symptom-free period (Andrews et al 2007, Pai et al 2017). Trauma- and Stressor-Related Disorders, as the latest classification introduced in the current diagnostic manual (DSM-5 2013), further reflect this difficult situation that the resulting disorders inconsistently embrace a wide array of symptoms even though they are common in the defining feature which includes the involvement of an adverse event (Pai et al 2017). Since the combination of psychological therapy and pharmacotherapy does not provide a more efficacious treatment than psychological therapy alone (Hetrick et al 2010, Mataix-Cols et al 2017), a primary question has been how a psychopathological model could account for PTSD development (McFarlane 2010). Several psychological programs were demonstrated as efficacious first-line treatments for PTSD (Beck 2011, Schnyder & Cloitre 2015), but not during the incubation period. Additionally, the risk of worsening PTSD symptoms remains (Bryant et al 2013, Monson et al 2012). Although the mechanisms underlying these psychological therapies are largely speculative and rather not amenable to scientific inquiry (Schnyder & Cloitre 2015), a core belief shared across various hypotheses is to view PTSD as an association between trauma-induced states such as fear memory, increased anxiety, and social withdrawal (Bryant et al 2017, Ehlers & Clark 2000, Hayes et al 2012, Siegmund & Wotjak 2006, Zoladz & Diamond 2013). This view has further been presumed in explaining PTSD development over the incubation period (Bryant

et al 2017, Ehlers & Clark 2000, Siegmund & Wotjak 2006). Complex developmental trajectories of PTSD symptoms were demonstrated with associated physiological and environmental regulators (Bryant et al 2013), yet the scientific support for underlying psychological mechanism is still absent.

To identify psychopathological mechanism underlying stress incubation (Figure 2.2A) requires an experimental assay with purely psychosocial manipulations on controlled subjective experiences and a homogeneous genetic background. Laboratory rodents are widely researched model systems with rich empirical evidence of their validity in neuroscience, genetics, and pharmacology of stress (Calhoon & Tye 2015, Cryan & Holmes 2005, Kaouane et al 2012, Tovote et al 2015). Behavioral paradigms that simulate PTSD were established to expose the mechanistic and causal insights of long-term fear memory following acute physical stress (Balogh et al 2002, Philbert et al 2011) and learned depression after a prolonged period of repeated social defeat, either directly (Golden et al 2011) or through witnessing (Patki et al 2014, Sial et al 2016). While similar observations of a delayed period before showing substantial PTSD-like behaviors were reported in a relatively small number of experimental paradigms (Davis 1989, Pamplona et al 2011, Tsuda et al 2015, Warren et al 2013), there have been no studies that systematically and quantitatively address this important developmental process. On the other hand, behavioral studies revealed that laboratory rodents engage in advanced social behaviors within their cognitive capacities and share similar psychological states as human (Bartal et al 2011, Bartal et al 2014, Burkett et al 2016, Smith et al 2016). Yet, the capability of these animal model systems to imply human complex psychobehavioral development in psychiatry remains unclear. By combining behavioral scenarios, analytic methods, and theoretical hypotheses, here I scoped for a novel research approach to achieve implications about human PTSD psychological developments from psychobehavioral experiments in laboratory mice.

2.2 Methods

All animal experiments were approved by the Institutional Animal Care and Use Committee (IACUC) in the animal facility at the Okinawa Institute of Science and Technology (OIST) Graduate University, accredited by the Association for Assessment and Accreditation of Laboratory Animal Care (AAALAC).

2.2.1 Study design

Sample size. No statistical methods were used to predetermine sample sizes. Animal numbers were determined based on previous studies.

Rules for stopping data collection. Partner mice were expected to get minor injuries from aggressor mice during aggressive encounters, which normally should be through attack bites on the dorsal side of posterior trunk (Takahashi et al 2015). The aggressive encounter and all further experiments were terminated once (i) the partner mouse showed severe bleeding or ataxia, or (ii) the aggressor mice showed abnormal attack bites on any other body part. Partner mice that reached the criteria (i) were euthanized. Aggressor mice that reached the criteria (ii) were terminated its usage in any further experiments. If any aggressive sign (sideways threat, tail rattle, pursuit, and attack bite) was shown by the partner mouse, all further experiments with the partner mouse, aggressor mouse, and observer mouse were terminated.

Data inclusion/exclusion criteria. No data was excluded.

Outliers. No outliers were defined.

Selection of endpoints. The endpoints were prospectively selected.

Replicates. All behavioral tests were conducted in quintuplicate to octuplicate sampling replicates. All behavioral tests were conducted in single experimental cohorts. All other records were conducted in quadruplicate to septuplicate experimental cohorts.

Research objectives. The goal of this work is to identify diverse psychological aspects, temporal patterns, and associations of behavioral development in mice after a single trauma induction. Pre-specified hypotheses state that (i) internal psychological development is already represented in behavioral details during early post-traumatic phase, while (ii) an association among trauma-induced states such as fear memory, increased anxiety, and social withdrawal explains PTSD-like behavioral development. All other hypotheses were suggested after initiation of the data analyses.

Research subjects or units of investigation. 8-week-old male C57BL/6J mice, 16-week-old female C57BL/6J mice, and 20-week-old or older male Slc:ICR mice were used.

Experimental design. I approached the research goal by developing a novel mouse model of psychosocial trauma under highly controlled conditions (psychosocial manipulations, subjective experiences, and genetic background) and by applying fine-scale analysis to standard behavioral tests. To induce acute witnessing trauma, a pair-housed mouse observed how its partner got bullied by a larger, aggressive mouse on the day of trauma induction. After this trauma, the observer mouse was isolated and developed behavioral differences compared to control mice in the ensuing weeks. The control groups included (i) mice isolated without experiencing trauma induction, (ii) mice isolated after observing how a stranger mouse got bullied by a larger, aggressive mouse, (iii) mice isolated after exposed to a non-aggressive stranger mouse, and (iv) mice which were not isolated after observing how its partner got bullied by a larger, aggressive mouse. The behavioral tests included the light-dark box test, elevated plus-maze test, open field test, locomotor activity test, active social contact test to a female stranger, active social contact test to a male stranger, and partner-revisiting test.

Randomization. Mice were from different litters. Mice were randomly paired. A focal mouse was randomly selected from each pair of mice. Mice were randomly

allocated into experimental groups. Testing order among groups was counterbalanced. Strangers and aggressors were randomly assigned.

Blinding. The investigator was blinded to behavioral outcomes but not to group allocation during data collection and/or analysis.

2.2.2 Overview

In total, 336 male C57BL/6J mice (CLEA Japan, Inc.), 36 female C57BL/6J mice (CLEA Japan, Inc.), and 28 male Slc:ICR mice (Japan SLC, Inc.; retired from breeding) were used in this study. In CLEA Japan, nursing females were individually housed (CL-0103-2; 165×234×118 mm), while pups were separated on P21 according to gender and housed ≤15 mice per cage (CL-0104-2; 206×317×125 mm). Pups were re-arranged on P28 according to their weights and housed ≤13 mice per cage (CL-0104-2). Mice were shipped in boxes each with 10 – 30 mice to the OIST Animal Facility. In the OIST Animal Facility, mice were housed in 380×180×160-mm transparent holding cages (Sealsafe Plus Mouse DGM - Digital Ready IVC; Tecniplast Inc., Quebec, Canada) bedded with 100% pulp (FUJ9298101; Oriental Yeast Co., Ltd., Tokyo, Japan) under a 12-hr dark/light cycle (350-lux white light) at a controlled temperature of 22.7 – 22.9 ˚C, humidity of 51 – 53%, and differential pressure of -14 – -8 Pa with food and water available *ad libitum*. Circadian time (CT) is defined to start at mid-light period and described in a 24-hr format, i.e. light off at CT 6:00.

The experimenter and caretakers wore laboratory jumpsuits, lab boots, latex gloves, face masks, and hair nets when handling mice and performing experiments. Handling of mice during the dark cycle was done under dim red light and mice were transported in a lightproof carrier within the animal facility. For mice in experimental and control groups tested on the same dates, the testing order was alternated. Surfaces of experimental apparatuses were wiped with 70% ethanol in water and dry paper tissues after testing each mouse to remove olfactory cues. Each mouse was only used for one behavioral test (in total 4 records with intervals of 6 – 21 days) to avoid

confounded results due to cross-testing and to minimize measurement effects on its psychological development (Krishnan et al 2007).

2.2.3 Pre-traumatic period (Day-21 to Day0)

To establish partnerships between mice, a male C57BL/6J mouse (focal mouse; 8 weeks) was pair-housed with another male C57BL/6J mouse (partner mouse; 8 weeks) for 3 weeks (Day-21 to Day0, with trauma induction on Day0). The partner was initially marked by ear punching. The holding cage was replaced once per week, with the last change 3 days before the traumatic event (Day-3).

To establish the territory of an aggressor mouse in its homecage, an Slc:ICR mouse (aggressor mouse; ≥20 weeks) was pair-housed with a female C57BL/6J mouse (female mouse; 16 weeks) for 3 weeks (Day-21 to Day0). The holding cage was replaced with a clean one once a week, with the last change one week before the traumatic event (Day-7).

Aggression level of aggressors was screened on Days -5, -3, -1 through intruder encounters (Miczek & O'Donnell 1978) toward different screening mice to determine appropriate aggressors to be used for trauma induction on Day0. Aggression screening was carried out in the behavior testing room at 22.4 – 23.0 ˚C, 53 – 58% humidity, -4 – -3 Pa differential pressure, and 57.1 dB(C) ambient noise level during the light period (CT 4:00 – 6:00) with 350-lux white light. After the female and pups with the aggressor were taken out of their homecage and kept in a clean holding cage in the behavior testing room, a 3-min aggression screening was started after a male C57BL/6J mouse (screening mouse; 10 weeks) was brought into the homecage of the aggressor, followed by covering the cage with a transparent acrylic lid. During screening, the aggressor freely interacted with the screening mouse. The aggressor was brought back to the holding room after the screening mouse was taken away from the aggressor's homecage and the female and pups were brought back to its homecage right after screening. Aggressors were selected for trauma induction on Day0 if they

showed biting attacks on all of these screening days and the latencies to the initial bites on Day-3 and Day-1 were less than 20 s.

2.2.4 Trauma induction (Day0)

The following experimental assay emotionally introduced an acute traumatic experience in mice through a social process. The setup was the aggressor's homecage, divided into an 80×180-mm auditorium zone and a 300×180-mm battle arena by the insertion of a stainless-steel mash with 8×8-mm lattices. The cage was covered with a transparent acrylic lid. The behavioral procedure was carried out in the behavior testing room during CT 4:00 – 6:00, with 3 – 5 experiments done in parallel.

After the female and pups with the aggressor were taken out of their homecage, a divider was inserted into the aggressor's homecage, allowing the aggressor to freely behave in the battle arena, but not to enter the auditorium zone. A 5-min aggression encounter session started after the focal mouse was brought to the auditorium zone and its partner to the battle arena. Tail rattling counts of the focal mouse during aggressive encounter were recorded by experimenter. The aggressive encounter session was followed by a 5-min stress infiltration session, in which the partner was brought to the focal mouse in the auditorium zone, while the aggressor remained in the battle arena. Right after the stress infiltration session, both focal mouse and its partner were brought back to their homecage in the behavior testing room for a 10-min resting period. The procedure was repeated 5 times with different aggressors. During each resting session, the aggressor stayed in its homecage without the divider before its next intruder encounter. Each aggressor had 3 – 5 encounters with resting periods of 10 – 30 min. After the 5th aggression encounter session, the focal mouse was placed back in its homecage where the nest had been razed, and brought back to the holding room. Partners from different pairs were brought to a new holding cage and housed in groups of 3 – 5 per cage. Right after the last intruder encounter for each

aggressor, the female and pups were brought back to the homecage and returned to the holding room together with the aggressor.

2.2.5 Post-traumatic period (Day0 to Day28)

To investigate the behavior of focal mice after trauma induction (now called Traumatized mice), they were housed individually for 4 weeks after the procedure (Day0 to Day28). No environmental enrichment was provided and the holding cage was not changed during social isolation.

2.2.6 Control experiments

To differentiate behavioral consequences of the emotionally traumatic experience from consequences of social isolation, a control group of mice had their partners taken away and their nests razed during body weighing on Day0 without trauma induction (Control mice, Figure 2.1A).

To test the influence of social relationship on the emotionally traumatic experience, a control group of mice witnessed the traumatic events toward stranger mice of the same strain, gender, and age instead (Stranger-observing mice, Figure 2.1B). In each iteration of the aggression encounter, stress infiltration, and resting period, a different stranger mouse was presented.

To identify the impacts of aggression during trauma induction, a control group of mice experienced exposure to strangers of the same strain, gender, and age, instead of the aggressor mice for trauma induction (Stranger-exposed mice, Figure 2.1C).

To examine the effects of social support on the emotionally traumatic experience, a control group of mice was kept pair-housed with their attacked partners after trauma induction (Buffered mice, Figure 2.1D).

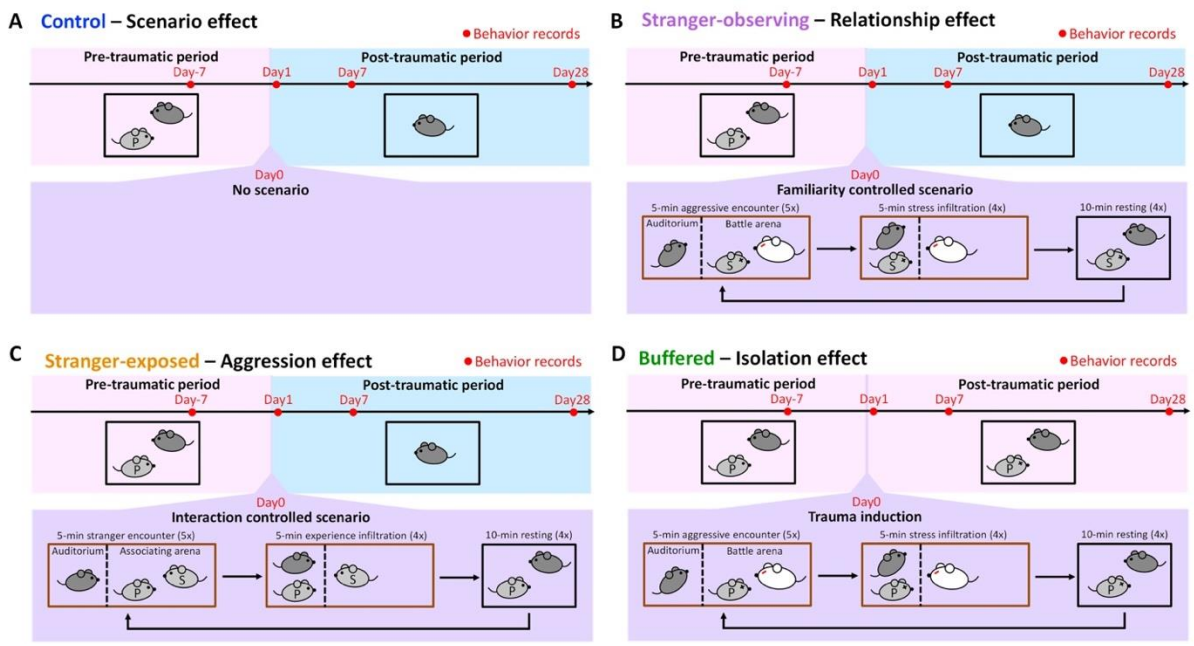

Figure 2.1. Control experiments demonstrate psychosocial factors that determined the behavioral developments. **(A)** Experiments of Control mice which had no experience of trauma induction identified the scenario effect in the behavioral paradigm. **(B)** Experiments of Stranger-observing mice which had witnessing experience of trauma that happened to strangers, rather than to their pair-housed partners, identified the relationship effect in the behavioral paradigm. **(C)** Experiments of Stranger-exposed mice which had experience of social interactions without witnessing stress from strangers identified the aggression effect in the behavioral paradigm. **(D)** Experiments of Buffered mice which were pair-housed with their partners after trauma induction identified the isolation effect in the behavioral paradigm.

2.2.7 Body mass and nest wall height

In the holding room, body masses of all individuals were recorded on Days -7, 0, 1, 7, 28, while the heights of nest walls built by each individual were recorded on Days 1, 7, 28. The height of the nest wall was measured with 5-mm resolution using a transparent acrylic ruler, while the mouse was weighed with 0.01-g resolution on a balance. Mice were placed back in their homecages right after recording.

2.2.8 Light-dark box test

The light-dark box test is an experimental assay to measure anxiety in rodents (Crawley & Goodwin 1980), designed to evaluate their natural aversion to brightly lit areas against their temptation to explore. The light-dark box setup consisted of two connected 200×200×250-mm non-transparent PVC boxes, separated by a wall with a 50 ×30-mm door. The boxes were covered with lids with white and infrared LED light illumination for the light and dark areas, respectively, and CCD cameras in the centers (4-chamber system; O'Hara & Co., Ltd., Tokyo, Japan). The floors of the boxes were white, while the walls of the boxes were white for the light area and black for the dark area. Uniform illumination in the light area was 550 lux. Behavioral tests were carried out on Days -7, 1, 7, and 28 in the behavior testing room at 22.7 – 23.0 ˚C, 51 – 54% humidity, -11 – -9 Pa differential pressure, and 53.6 dB(C) ambient noise level during dark period (CT 6:00 – 8:00).

After habituation for 10 min individually in the homecage in the behavior testing room in darkness, the focal mouse was transferred to the dark area through a 50×50-mm side door. A 5-min behavior record was started right after the side door of dark area was closed and the door between light and dark areas was opened. Locomotion was recorded 2-dimensionally at 15 Hz from top-view with CCD video cameras. Right after recording, the mouse was returned to its homecage, and brought back to the holding room.

2.2.9 Elevated plus-maze test

The elevated plus-maze test is an experimental assay to measure anxiety in rodents (Pellow et al 1985), designed to evaluate their natural fear of falling and exposure against their temptation to explore. The elevated plus-maze setup consisted of a gray PVC platform raised 500 mm above the ground (single maze system; O'Hara & Co., Ltd.). The platform was composed of a 50×50-mm square central platform, two opposing 50×250-mm open arms, and two opposing 50×250-mm closed arms with 150-mm semi-transparent walls. Each of the two open arms emanated at 90° to each of the two closed arms, and *vice versa*. The apparatus was installed in a soundproof box with white fluorescent lamp illumination (20 lux) and ventilators. Behavioral tests were carried out on Days -7, 1, 7, 28 in the behavior testing room at 22.8 – 23.0 ˚C, 53 – 56% humidity, -13 – -11 Pa differential pressure, and 52.1 dB(C) ambient noise level during dark period (CT 8:00 – 10:00).

After habituation for 10 min individually in the homecage in the behavior testing room in darkness, the focal mouse was brought to the central platform of the elevated plus-maze, facing the open arm on the opposite side from the door of the soundproof box. A 5-min behavior recording was started right after the door of the soundproof box was closed. Locomotion was recorded 2-dimensionally at 15 Hz from top-view with a CCD video camera installed above the center of the central platform. Delineated entrances to open and closed arms were defined at 50 mm from the center of the central platform. Right after recording, the mouse was placed back in its homecage, and brought back to the holding room.

2.2.10 Open field test

The open field test is an experimental assay to measure anxiety in rodents (Hall & Ballachey 1932), designed to evaluate their spontaneous activity under a gradient of spatial uncertainty (high in the field center and low along the walls and at the corners of the field). The open field setup consisted of a 400×400×300-mm non-transparent

gray PVC box with no cover, installed in a soundproof box with white LED light illumination and ventilators (2-chamber system; O'Hara & Co., Ltd.). Behavioral tests were carried out on Days -7, 1, 7, 28 in the behavior testing room at 22.8 – 23.0 ˚C, 53 – 56% humidity, -13 – -11 Pa differential pressure, and 56.7 dB(C) ambient noise level during dark period (CT 8:00 – 10:00).

After habituation for 10 min individually in the homecage in the behavior testing room in darkness, the focal mouse was brought to the center of the open field arena under 20-lux uniform illumination, facing the wall on the opposite side from the door of the soundproof box. A 5-min behavior recording was started right after the door of the soundproof box was closed. Locomotion was recorded 2-dimensionally at 15 Hz from top-view with a CCD video camera installed above the center of the open field arena. Vertical activity of exploratory rearing behavior was recorded by the blocking of invisible infrared beams created and detected by photocell emitters and receptors, respectively, positioned 60 mm high on the walls of the open field box. A delineated center region was defined as the central 220×220 mm area. Right after recording, the mouse was placed back in its homecage, and returned to the holding room.

2.2.11 Locomotor activity test

The locomotor activity test is an experimental assay to measure spontaneous activity of rodents in an environment without an experimentally designed stressor. The locomotor activity setup consisted of a 200×200×250 mm non-transparent covered PVC box with infrared LED illumination and a CCD camera in the center (the dark area of the light-dark box setup, while the door between the light and dark areas was closed and fixed). The floor of the box was embedded with bedding material from the homecage of the focal mouse, while the walls of the box were black. Behavioral test was carried out on Days -7, 1, 7, 28 in the behavior testing room at 22.7 – 23.0 ˚C, 51 – 54% humidity, -11 – -9 Pa differential pressure, and 53.6 dB(C) ambient noise level during dark period (CT 6:00 – 8:00).

After habituation for 30 min individually in the behavior testing box, a 1-hr behavior recording was started. The behavior testing box was not covered completely in order to allow air circulation. Locomotion was recorded 2-dimensionally at 15 Hz from top-view with the CCD video camera. Right after recording, the mouse was returned to its homecage, and brought back to the holding room.

2.2.12 Active social contact test

The active social contact test is a 2-session experimental assay to measure social motivation in rodents (Berton et al 2006). The setup consists of a 400×400×300-mm non-transparent gray PVC box with no cover, installed in a soundproof box with 20-lux white LED illumination and ventilators. A $60 \times 100 \times 300$-mm stainless-steel chamber with wire grid sides was placed in the center of the wall on the opposite side from the door of the soundproof box. The wire grid had 8×8 mm lattices at a height of 10 – 60 mm from the bottom. An ultrasound microphone (CM16/CMPA; Avisoft Bioacoustics, Glienicke, Germany) with an acoustic recording system (UltraSoundGate; Avisoft Bioacoustics) was hung outside the chamber, 100 mm above the ground. Behavioral tests were carried out on Days -7, 1, 7, 28 in the behavior testing room at 22.8 – 23.0 ˚C, 53 – 56% humidity, -13 – -11 Pa differential pressure, and 56.7 dB(C) ambient noise level during dark period (CT 8:00 – 10:00).

The social target used for active social contact tests was either a male or a female C57BL/6J mouse (18 weeks), pair-housed with a partner of the same strain, gender, and age for more than 2 weeks before the tests. The social target was adapted to the experimental protocol one day before the tests in the behavior testing room during dark period (CT 8:00 – 9:00): After habituation for 5 min individually in the homecage in the soundproof box under 20-lux uniform illumination, the social target was brought into the chamber in the open field arena under 20 lux uniform illumination. A male C57BL/6J mouse (11–16 weeks; from partners of Control mice in previous experiment) was then brought to the open field arena for a 2.5-min spontaneous

exploration and interaction with the social target. The social target was then brought back to its homecage in the soundproof box under 20-lux uniform light for a 5-min rest. The social interaction procedure was repeated with a different male C57BL/6J mouse right afterward. After the social target had interacted with 4 different mice, it was returned to its homecage and brought back to the holding room.

On testing days, after 10-min habituation individually in its homecage in the behavior testing room in darkness, the first session of the active social contact test started by placing the focal mouse at the center of the open field arena under 20-lux uniform light, facing the empty chamber. A 2.5-min behavior recording started right after the door of the soundproof box was closed. Locomotion was recorded 2-dimensionally at 15 Hz from top-view with a CCD video camera installed above the center of the open field arena. Ultrasonic vocalization was recorded at 250 kHz. In the second session of the active social contact test, which followed the first session, the social target was brought into the chamber. Another 2.5-min behavior recording started as soon as the door of the soundproof box was closed. Right afterward, the focal mouse was returned to its homecage and brought back to the holding room.

The focal mouse experienced active social contact tests with different social targets on different recording days (Days -7, 1, 7, 28), while different focal mice were tested with the same social target on the same recording day (5 – 10 records). The social target remained in its homecage in a soundproof box under 20-lux uniform illumination before and between each test. A delineated interaction zone was taken as the region within 80 mm of the edges of the chamber. Social approaches of the focal mouse poking its nose toward the social target were recorded manually using the event recording software, tanaMove ver0.09 (http://www.mgrl-lab.jp/tanaMove.html).

2.2.13 Partner-revisiting test

The partner-revisiting test is a memory-based experimental assay to measure social bonding in rodents. The partner-revisiting setup was the uncovered homecage

of the focal mouse, installed in a soundproof box with white LED illumination and ventilators (O'Hara & Co., Ltd., Tokyo, Japan). The long sides of the homecage were parallel to the door of soundproof box. The partner-revisiting test was carried out on Day28 in the behavior testing room at 22.8 – 23.0 ˚C, 53 – 56% humidity, -13 – -11 Pa differential pressure, and 56.7 dB(C) ambient noise level during light period (CT 4:00 – 6:00) with 350-lux light intensity.

The previously separated partner of the focal mouse, being a social target in the test, was initially sedated with 3%v/v isoflurane in oxygen, and then anesthetized by intraperitoneal (i.p.) injection of a mixture of medetomidine (domitor, 3%v/v in saline, 0.3 mg/kg), midazolam (dormicum, 8%v/v in saline, 4 mg/kg), and butorphanol (vetorphale, 10%v/v in saline,5 mg/kg). Also, a stranger mouse (15 weeks; a separated partner of a Traumatized or Buffered mouse for testing a Control, Stranger-observing, or Stranger-exposed mouse, and *vice versa*) was anesthetized as an alternative social target. Both anesthetized mice were kept on a heating pad at 34˚C (B00O5X4LQ2; GEX Co., Ltd., Osaka, Japan) to maintain their body temperatures before the test.

The focal mouse was brought to a clean, uncovered holding cage in the soundproof box under 50-lux uniform illumination for 5-min habituation, while its homecage was placed in another soundproof box under 50-lux uniform light. During habituation of the focal mouse, the anesthetized social targets were injected with atipamezole hydrochloride (antisedan; 6%v/v in saline for 0.3 mg/kg, i.p.) to induce recovery from anesthesia. During the waking-up period, the social targets were still immobilized and not able to actively interact with the focal mouse during the following recording, but showed enough social cues to be attractive for the focal mouse. The immobilized social targets were then placed in the homecage of the focal mouse with their nose pointing toward the center of the short side of the wall (10 mm of nose-to-wall distance) with their bellies facing the door of the soundproof box. After habituation, the focal mouse was brought to the center of its homecage, facing the long side of the homecage wall on the opposite side from the door of soundproof box. A

10-min behavior record started right after the door of the soundproof box was closed. Locomotion was recorded 2-dimensionally at 15 Hz from top-view with a CCD video camera installed above the center of the homecage. Right after recording, social targets were taken out of the focal mouse's homecage and the focal mouse was brought back to the holding room.

Social contacts including sniffing, allogrooming, and pushing of the focal mouse toward each of the social targets were recorded manually using the event recording software, tanaMove ver0.09 (http://www.mgrl-lab.jp/tanaMove.html).

2.2.14 Video image process

Video image data was processed using custom scripts written in MATLAB R2015b (MathWorks). Each video frame from a recorded AVI video file was read as a 2-dimensional matrix with an 8-bit gray scale. Each of these matrices was then divided by a background matrix read from a TIF image file of the background taken before bringing the test mouse to the setup. The centroid of the area with non-one values in each matrix ratio was taken as the position of the mouse at this specific time point. Speed was calculated as the distance between temporally adjacent positions multiplied by 15 (15-Hz recording). Freezing periods were sorted out if the area of the mouse body between temporally adjacent frames was less than 20 mm^2.

2.2.15 Audio signal process

Audio signal data was processed with custom scripts written in MATLAB R2015b (MathWorks). Each recorded WAV audio file was read and transformed into a spectrogram using fast Fourier transform with non-overlapping 0.4-ms time windows. To identify the time segments with ultrasonic vocalization signals, recordings were thresholded at a power spectral density (PSD) ≥-75 dB/Hz, and time segments with averaged PSD between 0–50 kHz higher than that between 50–120 kHz were removed. The duration of remaining time segments was calculated.

2.2.16 Statistical analysis

Numerical data were analyzed with custom scripts written in MATLAB R2015b (MathWorks). Statistical significance of the difference between 2 mean values was estimated with two-tailed, two-sample Student's *t*-test. Statistical significance of the difference between 2 median values (vocalization analysis; Figure 2.8) was estimated using one-tailed Mann–Whitney *U* test.

To capture fine-scale behavioral details of location within the light-dark box and the elevated plus-maze (Figure, 2.2C and 2.5A), I computed T(x), the cumulative probability of finding position ≤x, for each individual (light traces) for all measured locations (a collection of locations from all mice for the statistics). I then show the average across the control group (bold blue trace) and the Traumatized group (bold red trace). I compared the averages of each group with a two-tailed, two-sample Student's *t*-test and plot the resulting p-values, presented as -log(p), the negative logarithm of *p*-values. I also show the box plot (the minimum, lower quartile, median, upper quartile, and maximum) of -log(p) values collapsed across all measured locations. To capture the fine- scale behavioral details of speed, I followed a similar procedure as above, but with U(v), the cumulative distribution function of finding speed ≤v.

To evaluate the uncertainty of the percentage for each tail rattle count (Figure 2.10A), I created 10,000 bootstrapped data sets where each sample was randomly picked with replacement from the original data set. Each bootstrapped data set had the same sample size as the original data set. The standard error was taken as the standard deviation of the bootstrapped percentages for a tail rattle count. A similar procedure was carried out to evaluate the standard error of mean for the percentage of time spent in each behavior in the partner-revisiting test (Figure 2.10D), where each sample of the bootstrapped data sets was a set of the percentages of the three classified behaviors (partner concern, stranger concern, and non-social activity/sniffing at social targets) from a mouse record. Standard errors of means for other results were

estimated with the formula $\sigma/\sqrt{n}$, where σ is the sample standard deviation and n is the sample size.

2.3 Results

2.3.1 Evidence of stress development revealed by fine-scale behavioral analysis

To identify post-traumatic behavioral development with minimal physical impact and peri-traumatic contribution, I developed the following assay of acute witnessing trauma (Figure 2.2, B and C): Partnership between the male focal mouse and its male partner was established by housing them together for 3 weeks (Day-21 – Day0). During this pair-housing, the mice slept together in a single nest they built, and no aggressive interaction was observed. On Day0 (trauma induction), the focal mouse observed its partner being attacked by 5 different aggressor mice in succession (aggressive encounter), and stayed together with the attacked partner between each aggressive encounter (stress infiltration and resting). Importantly, the focal mouse only experienced the traumatic event by witnessing the attacks and via social communication, but not through any direct physical threat, such as attack bites and pursuits from either the aggressors or its partner. After the last aggressive encounter, the focal mouse (Traumatized mouse) was socially isolated for 4 weeks (Day0 – Day28). Behavior was tested on Days -7, 1, 7, and 28.

To differentiate behavioral consequences from the trauma induction and the effects of isolation, adaptation to the tests, and aging, a control group of mice were isolated from their partners on Day0 without trauma induction (Control mice). I found that Traumatized mice (n = 47) built nests with significantly higher walls than those constructed by Control mice (n = 47) after isolation (Figure 2.2D). Traumatized mice also increased their body masses in the late phase of the study (Figure 2.2E). While these differences could be alternatively explained [e.g. having better emotional stability and therefore nicer nests and better appetites *versus* manifesting protective responses of anxiety by hiding behind higher nest walls and engaging in anxiety-

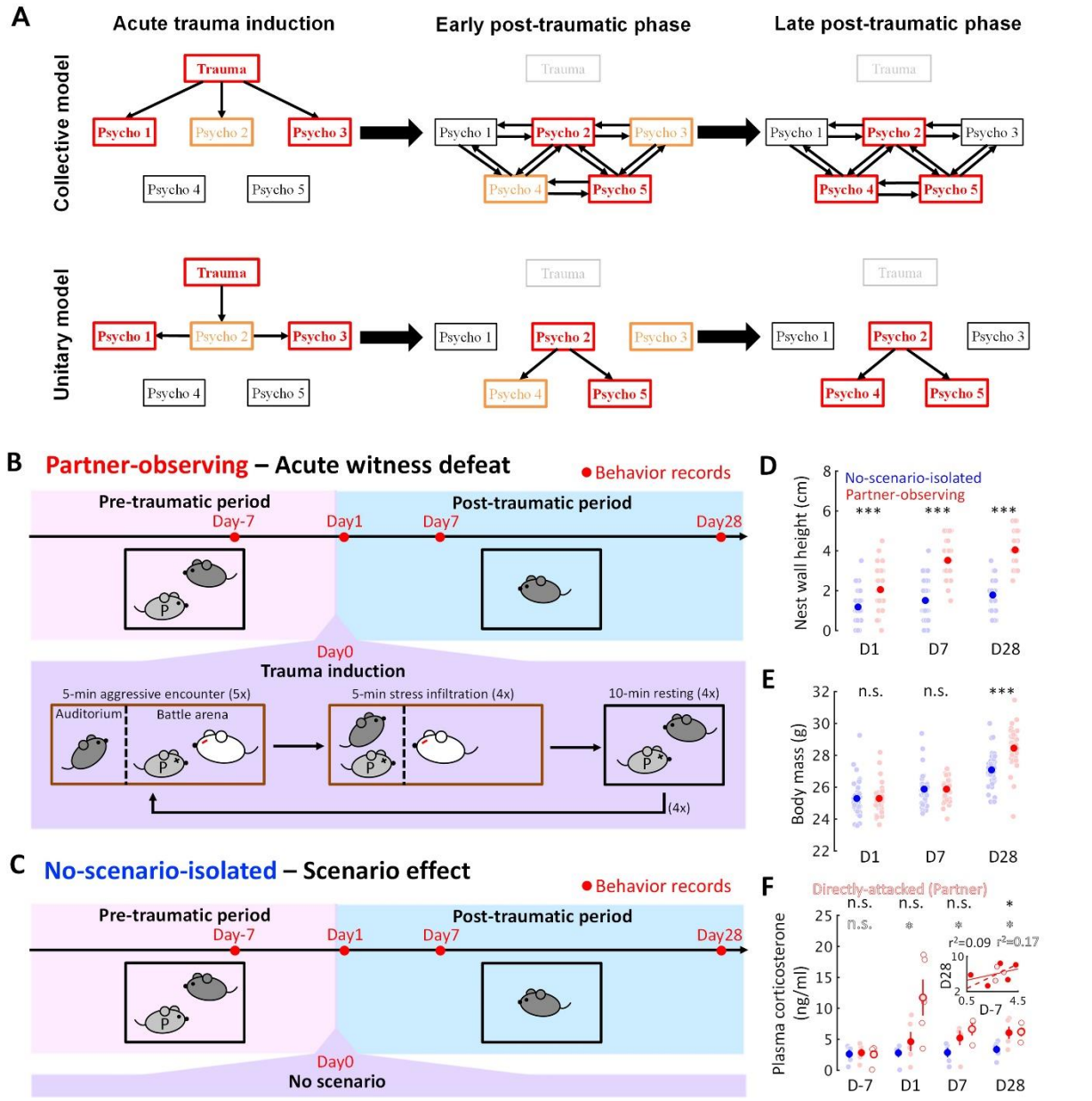

Figure 2.2. Acute induction of observational stress produces long-term and delayed effects on multiple behaviors and physical conditions. **(A)** Two competitive conceptual models explain the incubation process during post-traumatic stress development. Causal relations (arrows) among different psychological elements (Psycho #, a type of emotion or cognition) for stress development during different phases in the collective (top) and unitary (bottom) hypotheses. Orange and red represent medium and strong trauma-induced differences, respectively. Each psychological element can be inferred to an associative neural substrate of a corresponding neural circuit, and the trauma-induced neural difference can be taken as the difference between the post-traumatic and pre-traumatic neural dynamical states. **(B)** Paradigm inducing acute psychosocial trauma in mice (Partner-observing mice). Focal mouse

(dark gray; the Partner-observing mouse), partner mouse (light gray P), aggressor mouse (white), focal mouse's homecage (black), aggressor's homecage (brown), and wire-meshed divider (dashed line). **(C)** Experiments of No-scenario-isolated mice which had no experience of trauma induction identified the scenario effect in the behavioral paradigm. **(D)** Nest wall heights show long-lasting significant differences after trauma induction. **(E)** Body masses show significant delay difference after trauma induction. **(F)** Baseline plasma corticosterone levels show delay expression of long-lasting significant differences after trauma induction for both Partner-observing mice and their partners (Directly-attacked mice). The individual variation of this chronic impact was not predicted by the baseline plasma corticosterone levels before trauma. Light dots or lines, data of individual mice; deep dots or lines, means across populations; deep vertical lines, standard errors in the means; open circles, open words, or dashed lines, data with respect to Directly-attacked mice; n.s., $p \geq 0.05$; *, $0.01 \leq p < 0.05$; ***, $p < 0.001$;statistical significance of the difference in mean values was determined with a two-tailed, two-sample Student's t-test.

induced binge eating (Goto et al 2014, Otabi et al 2017)], they clearly indicated a long-term psychological effect of trauma. I further investigated measure a physiological indicator of observational stress, corticosterone concentrations in blood plasma (Figure 2.2F). Compared with No-scenario-isolated mice, Partner-observing mice showed higher baseline plasma corticosterone level after trauma, which reached statistical significance on Day28. The tendency of higher baseline plasma corticosterone level was also observed in Directly-attacked mice which had a more obvious baseline corticosterone increment during the early phase, supporting the interpretation that the observed behavioral difference may be behavioral phenotypes of stress.

To investigate the emotional states of Traumatized mice, I used standard behavioral testing setups. Although the general beliefs in identifying rodent emotionality in standard behavioral tests have been criticized (Ramos 2008), spontaneous behavior in a steady environment is arguably a representation of internal states such as emotion (Archer 1973). In humans, anxious behaviors show when facing unexpected events or uncertain situations (Grupe & Nitschke 2013). Behavioral tests for rodent anxiety-like reactions were therefore designed to evaluate their stress reaction against their willingness to explore (e.g. light-dark box and elevated plus-maze) or their activity under conditions with a gradient of uncertainty (e.g. open field). I first examined spontaneous behaviors in the light-dark box test (Figure 2.3; n = 8 mice for each group), where the stressor was a natural aversion to brightly lit areas (Kumar et al 2013). While the time spent in the light area did not differ significantly between Control and Traumatized mice on Day1, Traumatized mice spent more time in the light area than Control mice on Days 7 and 28 (Figure 2.3A, left panels). This result, as the first glance, suggests delayed expression of a chronic behavioral difference.

This result raised the following questions: (i) Did this behavioral difference start to develop immediately after the traumatic event or only after a delay? (ii) What comparative emotionality does this behavioral difference indicate? To answer the first

question, I examined the fine-scale positions of the mice in the light-dark box. Emotion dynamically maps internal states and external stimuli toward a set of corresponding behaviors, which should be represented in the probability distribution of behaviors that are shown. Based on spatial symmetry, I analyzed T(x), the cumulative probability distribution of time that the mouse spent at positions along the axis of the light-dark box (Figure 2.3A, top-right scheme and the equation, and middle panels for the results). I calculated significance levels [presented as -log of *p*-values, -log(p)] of T(x) between Traumatized and Control populations by computing position-dependent population means and applying a two-tailed, two-sample Student's *t*-test (Figure 2.3A, bottom-middle panels). Already on Day1, Traumatized mice showed differences in their spatial distribution, as they spent less time than Control mice at the far end of the dark area. This tendency increased with time: On Day7, Traumatized mice spent more time in the light area close to the door compared to Controls, and then on Day 28 additionally on the far side of the light area. Collapsed -log(p) distributions reveal the overall gradual increase in spatial preference differences (Figure 2.3A, right panel). Additionally, Traumatized mice showed more transfers between the boxes and shorter latencies until their first transfers from Day1 (Figure 2.3C), and maintained a higher locomotor speed compared to the gradually decreasing speed of Control mice (Figure 2.3B). These results indicate an onset and gradual increase of behavioral differences immediately following the trauma.

2.3.2 Development of different psychological components untangled in standard behavioral tests

These differences may reflect the hypo-sensitivity to sensory harm and hyper-activity, as characteristic of somatic anxiety in PTSD patients (Adler et al 2004, Cloninger 1988, Mostoufi et al 2014); however, they may also simply indicate that Traumatized mice became braver and more excited. To determine whether the differences could be attributed to chronic anxiety, I examined their behaviors in the

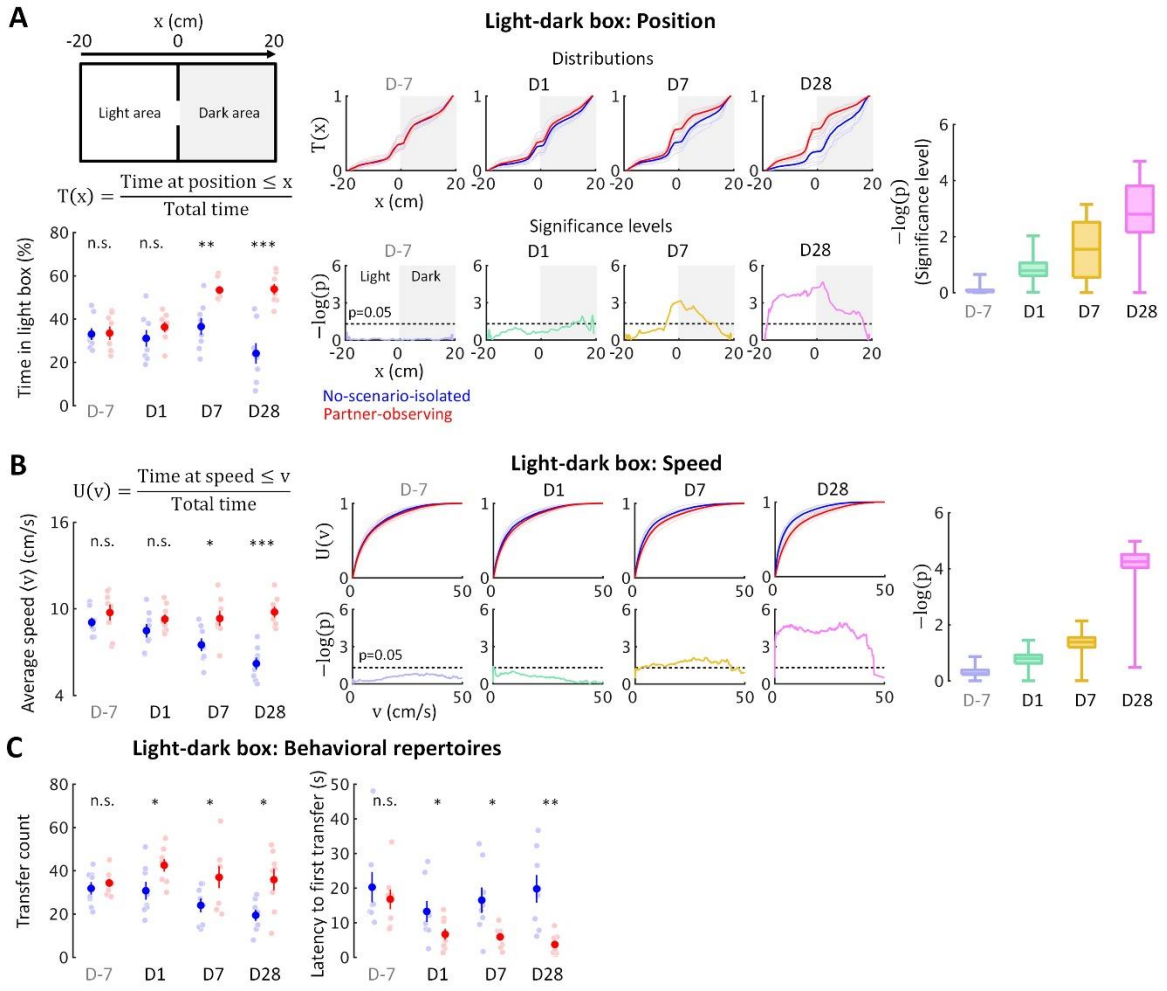

Figure 2.3. Fine-scale behavior alanalysis in light-dark box test detects the gradually developing process of the behavioral difference. (A) Light-dark box test quantified through the cumulative position probability T(x) along the light-dark axis (left). On average, Partner-observing mice (red) spent more time in the light area than No-scenario-isolated mice(blue) during the late post-traumatic period [T(0), bottom-left]. Spatially fine-scale behavioral analysis reveals significant differences between Partner-observing and No-scenario-isolated populations already in the early post-traumatic period (middle). For each position, I compute the mean T(x)across the No-scenario-isolated and Partner-observing populations and compute statistical significance through a two-population Student's t-test. These differences gradually increased, as evidenced by significance distributions collapsed across all positions (right; box plots show the minima, lower quartiles, medians, upper quartiles, and maxima). **(B)** I similarly quantified speed using the fine-scale cumulative distribution U(v)of having speed ≤v and I show the statistical analysis of population differences in U(v). Cumulative distribution functions of locomotion speed (U(v) of having speed ≤v) and corresponding significance

distributions provide an additional independent behavioral index that showed a gradually increasing differences of higher speed in Partner-observing mice. **(C)** Higher transfer counts and shorter latency to the first transfers in Partner-observing mice suggest their higher activity and exploratory motivation, respectively.

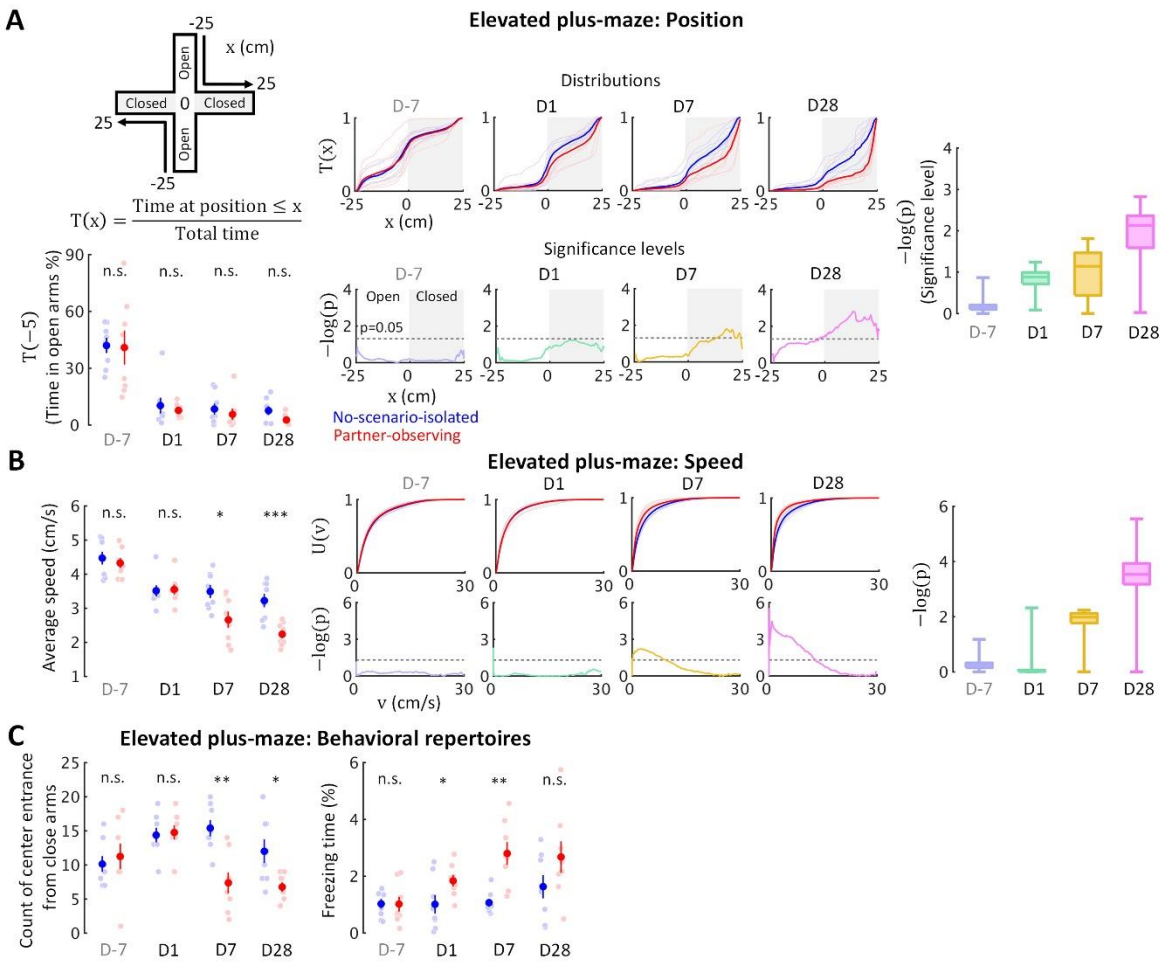

Figure 2.4. Behavioral testing in the elevated plus-maze demonstrates that stress incubation of anxiety caused the observed differences. **(A)** Partner-observing and No-scenario-isolated mice did not differ significantly in the time they spent in opened arms; however, spatial distributions show differences in preferred location between Partner-observing and No-scenario-isolated mice in the closed arms, which increased with time. **(B)** Cumulative distribution functions of locomotion speed and corresponding significance distributions show a gradually increasing differences of lower speeds in Partner-observing mice. **(C)** Less exploration from close arms to platform center and longer freezing time in Partner-observing mice suggest their stronger stress reactions.

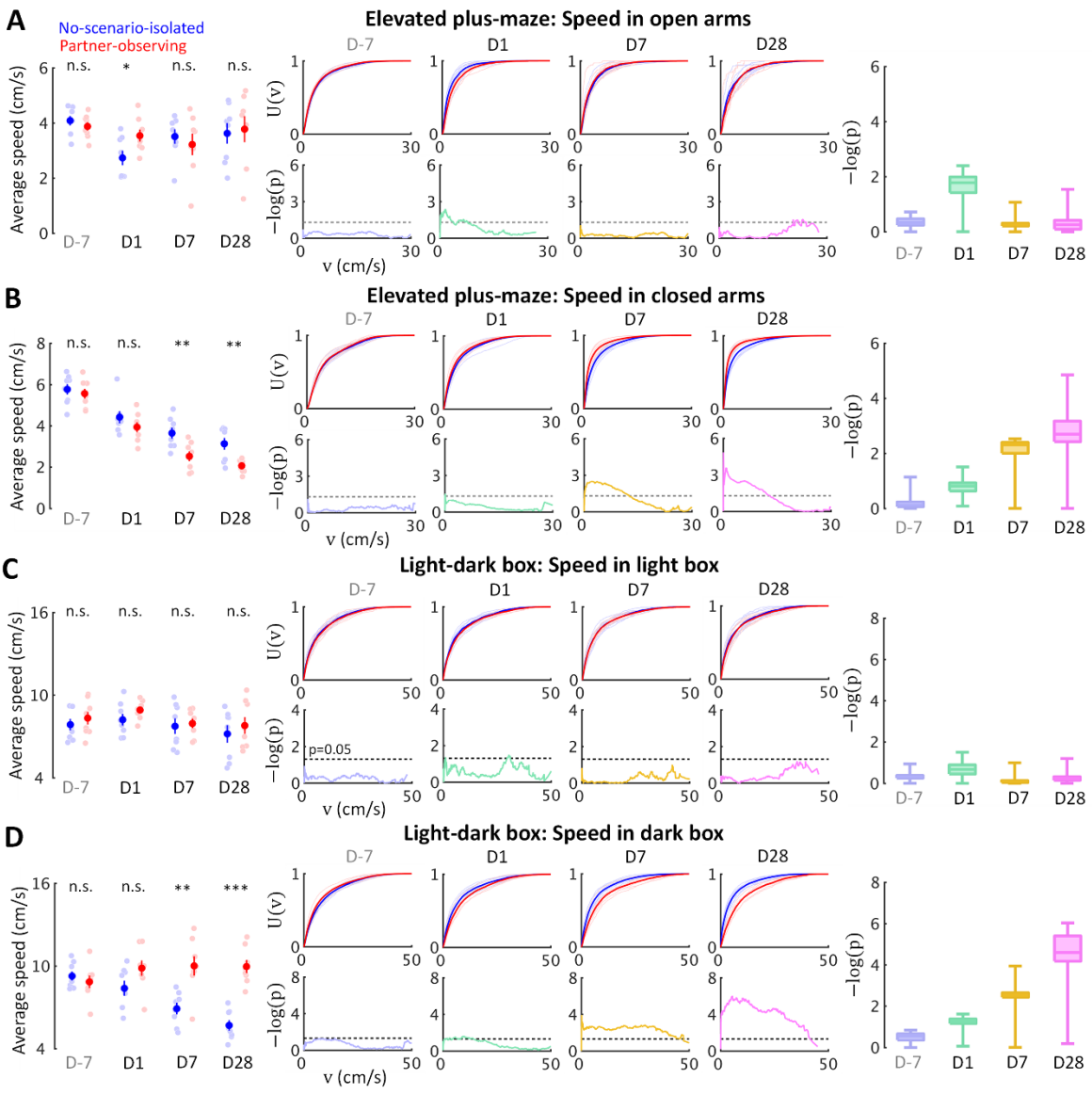

Figure 2.5. Gradually increasing anxiety and acute fear reaction were untangled in standard behavioral tests as different psychological components with distinctive developments. Locomotion speed shows acute difference only in stressor zones [open arms **(A)** and light area **(C)**], but incubated differences in stressor-free zones [dark area **(B)** and closed arms **(D)**].

elevated plus-maze test (Figure 2.4; n = 8 mice for each group). In this test, stressors included fear of falling and exposure, which accompanied both sensation and cognitive interpretation (Kumar et al 2013). Reactions of cognitive anxiety are expected to be opposite of those shown in somatic anxiety (Cloninger 1988). After first exposure on Day-7 and separation, mice spent only a fraction of the time in the open arms of the maze, but with no significant difference between Control and Traumatized mice (Figure 2.5A, left panels). However, Traumatized mice spent increasingly more time in the far end of the closed arms (Figure 2.4A, middle panels) and moved more slowly in the elevated plus-maze after trauma induction (Figure 2.4B) with longer periods of freezing and fewer entries to the central platform from the closed arms (Figure 2.3B). Together, this indicates a higher anxiety level and supports the hypothesis that behavioral differences are the result of a chronic anxiety. Gradually increasing differences between Control and Traumatized mice (Figure 2.4A, right panel; Figure 2.4B) further confirm that stress incubation of anxiety caused the observed differences.

To date, the controversy at the core of PTSD development that has not been directly addressed is the nature and source of internal psychological development. Rather than exploring determinants of a developmental phenotype or asking whether and how a behavioral output is generated via a conjoint process of multiple interpreting and evaluating systems (Calhoon & Tye 2015, Hayes et al 2012), the fundamental question asked for an internal psychological development is whether and how the alternation of an interpreting or evaluating system is dependent on the state of another interpreting or evaluating system. This dependence can be examined by comparing the observed results with the predictions according to possible causal scenarios for a pair of trauma-induced states in a unified framework (Oizumi et al 2016, Sapolsky 2002). To explore the developmental process of different psychological components, I next investigated the emotional basis further revealed in fine-scale behavioral distributions. In both tests, key incubation features were consistently more

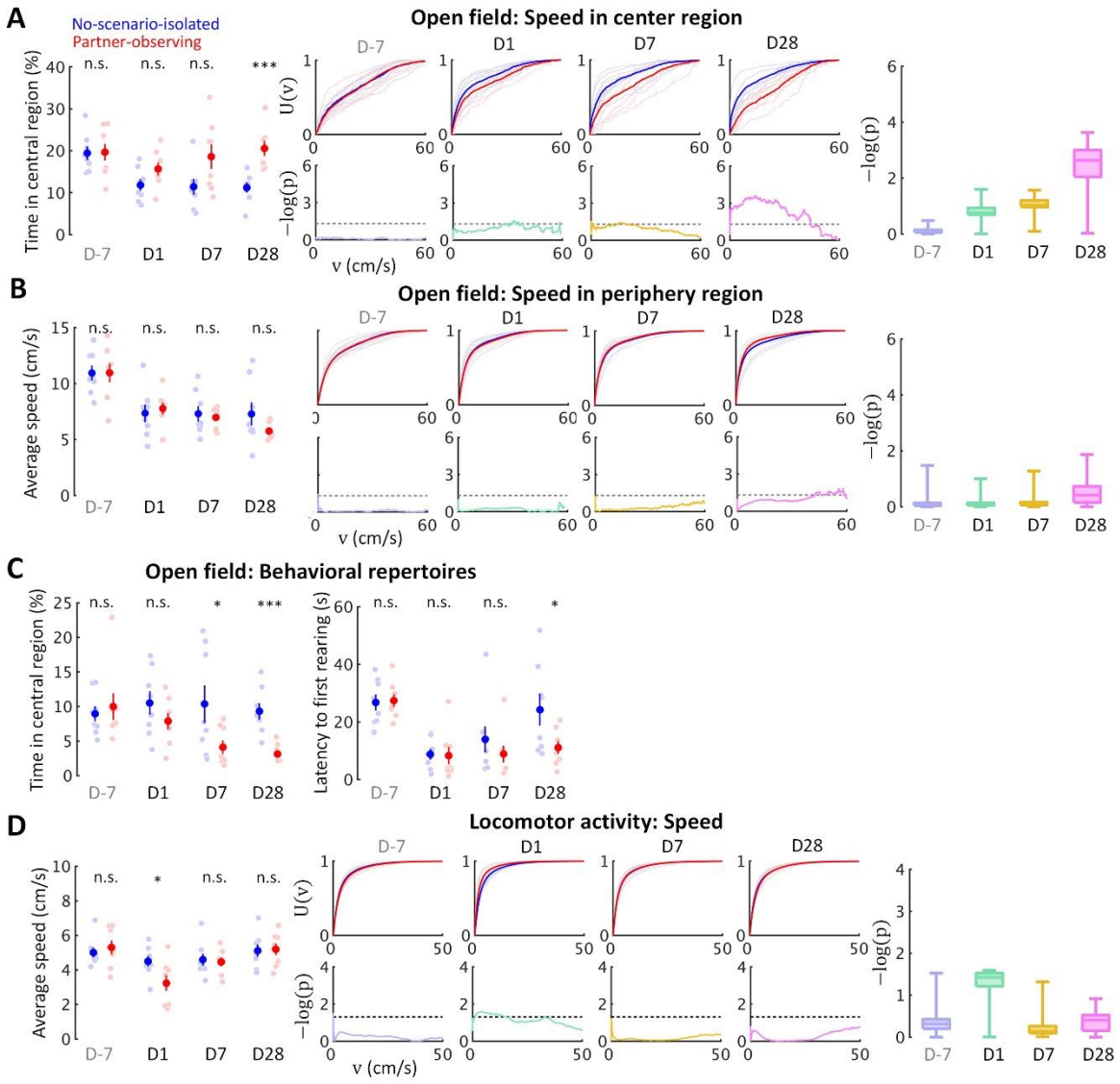

Figure 2.6. Behavioral testing in the open field test and locomotor activity test confirms distinctive psychological substrates and their corresponding development patterns. (A) Anxiety is evident in the open field test through a delayed onset of locomotor speed differences in the center region with higher spatial uncertainty. **(B)** The differences of locomotor speed observed in the center region did not occur in the periphery region with lower spatial uncertainty. **(C)** Less time spent in the central region by Partner-observing mice suggests their avoidance of a region with high special uncertainty, while shorter latency to their first rearing indicates their higher exploratory motivation. **(D)** In the locomotor activity test without stressors, acute effects of activity reduction recovered in the later post-traumatic period.

obvious within stressor-free zones (dark area and closed arms) than within stressor zones (light area and open arms), and thus the features of the behavioral response might change depending upon whether mice were under the stressor. To quantitatively investigate the differences between zones, I analyzed locomotor speed separately in stressor and stressor-free zones. As expected, two different behavioral patterns developed in the two zones: While speed differences consistently increased in stressor-free zones (Figure 2.4B, right panels; Figure 2.5, B and D), speed differences in stressor zones only showed acute increases on Day1 (Figure 2.4B, left panels; Figure 2.5, A and C). These results suggest that different psychological features were measured in the two zones, allowing further identification of association among different trauma-induced states.

In humans, fear is a response to a known threat with a magnitude that increases with the certainty of the threat, whereas anxiety is a response to uncertainty with a magnitude that increases with the uncertainty of a situation (Grupe & Nitschke 2013). Together with the presented demonstration of anxiety incubation (Figure 2.3A and 2.4A; Figure 2.3, A and B; Figure 2.4; Figure 2.5, A to D), I hypothesized that behavioral differences in stressor-free zones (closed to stressor) are the result of anxiety reactions to uncertainty, while acute stress reactions in stressor zones (under stressor) are the result of lasting fear responses from trauma induction. I examined mouse locomotor speed in uncertain and familiar environments separately using the open field test (Figure 2.6, A to C; n = 8 mice for each group) and the locomotor activity test (Figure 2.6D; n = 8 mice for each group), respectively. In the open field test, mice were exposed in a dimly lit environment with a gradient of spatial uncertainty from the field center (high uncertainty) to field boundaries (low uncertainty). In the locomotor activity test, mice were habituated in a dark environment with familiar cues of bedding materials from their homecages indicative of less environmental stress. Traumatized mice moved faster in the center region of the open field (Figure 2.6A), compared to Controls, and slower in the periphery (Figure 2.6B). The difference between groups increased

gradually and was greater in the center than in the periphery (Figure 2.6C). The avoidance of spatial uncertainty by Traumatized mice was also reflected in the shorter time they spent near the center (Figure 2.6A, left panel), but showed a shorter latency to the first rearing during the test (Figure 2.6B, right panel), which together suggests anxiety, instead of depression-like reactions with low exploratory motivation, as the causal emotional state. In contrast, Traumatized mice moved significantly more slowly on Day1 in the locomotor activity test, and recovered on Days 7 and 28 (Figure 2.6D). Notably, the two developmental patterns showed a consistent uncertainty-dependent manner and were measured across various behavioral tests. The patterns raised together in the acute phase, but one vanished when the other continued to increase in the later phase. These results support the hypothesized psychological features and further imply that delayed anxiety expression is not simply an expanded, sustained response of acute stress, thereby refuting a general belief (Andrews et al 2007, Bryant et al 2017, DSM-5 2013, DSM-III 1980, Ehlers & Clark 2000, Hayes et al 2012, Pamplona et al 2011, Schnyder & Cloitre , Siegmund & Wotjak 2006, Zoladz & Diamond 2013).

2.3.3 PTSD-like heterogeneous picture between emotionality and sociality

Emotional responses simplify and speed up animal reactions to complex external cues and are critical in social interactions (Anderson 2016). Impairment in social functioning is also considered in PTSD diagnosis (DSM-5 2013). To test potential effects of anxiety on sociality, I examined mouse social motivation in a two-session social test (Figure 2.7A, a non-social session followed by social session; n = 5 mice for each group). The social stimulus was either a female or a male stranger mouse. During the social session, Traumatized mice spent less time in social approaches of nose poking toward both female and male strangers, starting from Day1, and remained less social compared to Controls during the post-traumatic period (Figure 2.7B). In addition, less social vocalization was recorded during the female stranger test for

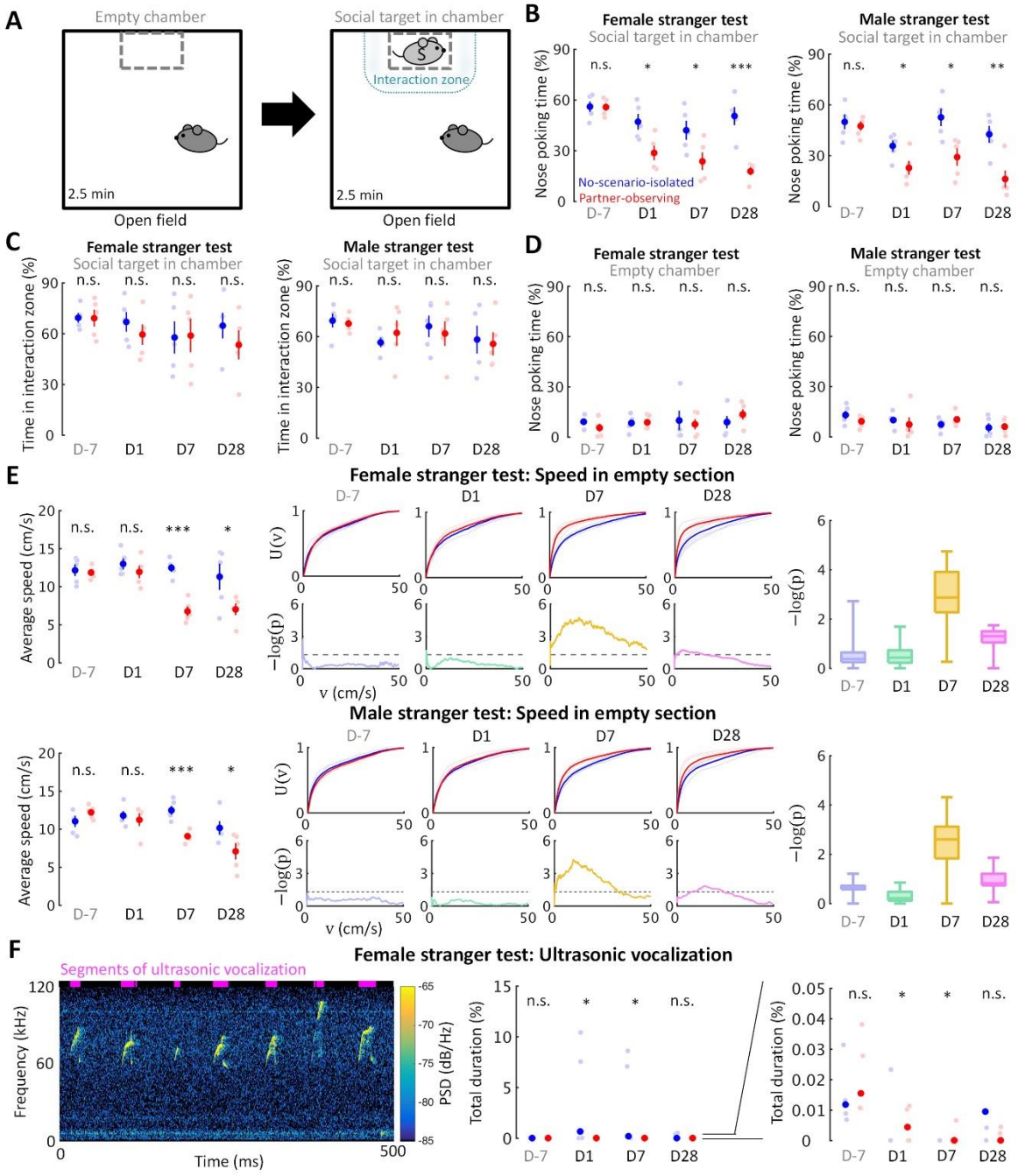

Figure 2.7. Acute psychosocial trauma decreases social interest. **(A)** The active social interaction test with consecutive non-social and social phases. During the social phase, motivation for social contact toward a stranger mouse (light gray S) was evaluated as the time spent for social approaches of nose poking and the time spent in the delineated interaction zone. **(B)** Partner-observing mice made fewer nose poking to both female (left) and male (right) strangers. **(C)** There was no significant difference in the time spent in the interaction zone during the social phase, suggesting a decrease of social interest instead of an active social

avoidance. **(D)** There was no significant difference in the time spent of nose poking during the non-social phase, confirming that the observed differences of nose poking time stemmed from a specifically social root. **(E)** Spectrogram of short but conspicuous ultrasonic vocalizations emphasizes a specific behavioral repertoire during the social session in the female stranger test of a No-scenario-isolated mouse on Day1. More vocalization was recorded from No-scenario-isolated mice than Partner-observing mice on Days 1 and 7. Reduced ultrasonic vocalization during the social session of the female stranger test in Partner-observing mice attests to diminished social communication. Note that data points greater than 0.05% are not visible in the right panel which zoom in the data of the middle panel to emphasize the data distributions in the range of 0–0.05%. Data points and median, one-tailed Mann-Whitney U test; PSD, power spectral density. **(F)** Partner-observing mice showed a delayed onset of reduction in locomotion speed during the non-social phase.

Traumatized mice (Figure 2.7F). The time they spent in the interaction zone around the social target, however, did not differ significantly from that of Control mice (Figure 2.7C). These results indicated a general and chronic social apathy that developed after the trauma. These observations are comparable to the diminished responsiveness in interpersonal relationships that begins soon after traumatic events as reported in PTSD patients (DSM-III 1980), rather than social avoidance, as expected in case of chronic anxiety generally considered in PTSD social withdrawal (DSM-5 2013, DSM-III 1980). In addition, onset of chronic social apathy from Day1 preceded the notable drop of spontaneous locomotor speed during the non-social session on Days 7 and 28 (Figure 2.7E). These results additionally suggest that post-traumatic social apathy is hard to explain in terms of emotional development due to its early onset, indicating that emotional and social consequences may arise independently from trauma induction.

2.3.4 Relationship-dependent behaviors suggesting affectional mechanism

To explore the key factor that determined the development of both emotionality and sociality required several control experiments (Figure 2.1). First, I compared behavioral developments of Control mice with a second control group of mice (Stranger-exposed mice) where the aggressor mice for trauma induction were replaced by non-aggressive strangers. Stranger-exposed mice did not show the developments of behavioral differences (Figure 2.8), suggesting that social aggression is necessary to induce stress developments. As Traumatized mice experienced the traumatic event purely psychosocially, partnership between mice served as a candidate variable with which to alter the emotional impact and coping strategy (Sandi & Haller 2015). Thus, I analyzed a third control group of mice (Stranger-observing mice) as each of them observed different stranger mice being attacked by different aggressors and stayed together with each stranger between aggressive encounters before isolation. Stranger-observing mice did not experience any physical stress from strangers or aggressors. Two notable behavioral differences during trauma induction were observed: While

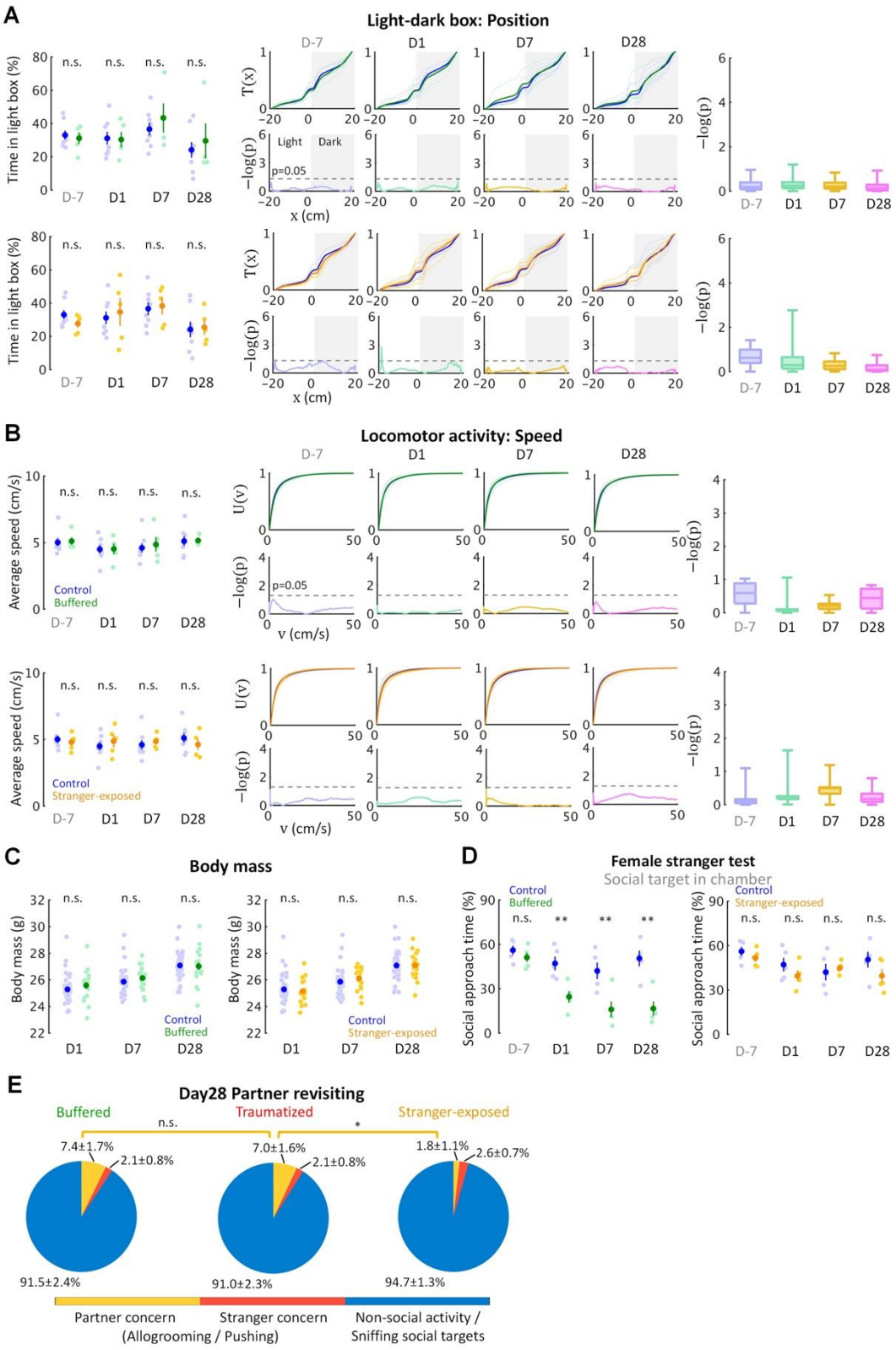

Figure 2.8. Control experiments identify distinctive psychological determinates for stress developments of emotionality and sociality. Emotionality interpreted from **(A)** the light-dark box test, **(B)** locomotor activity test, and **(C)** body mass measurement. Sociality interpreted from **(D)** the active social contact test and **(E)** partner revisiting test.

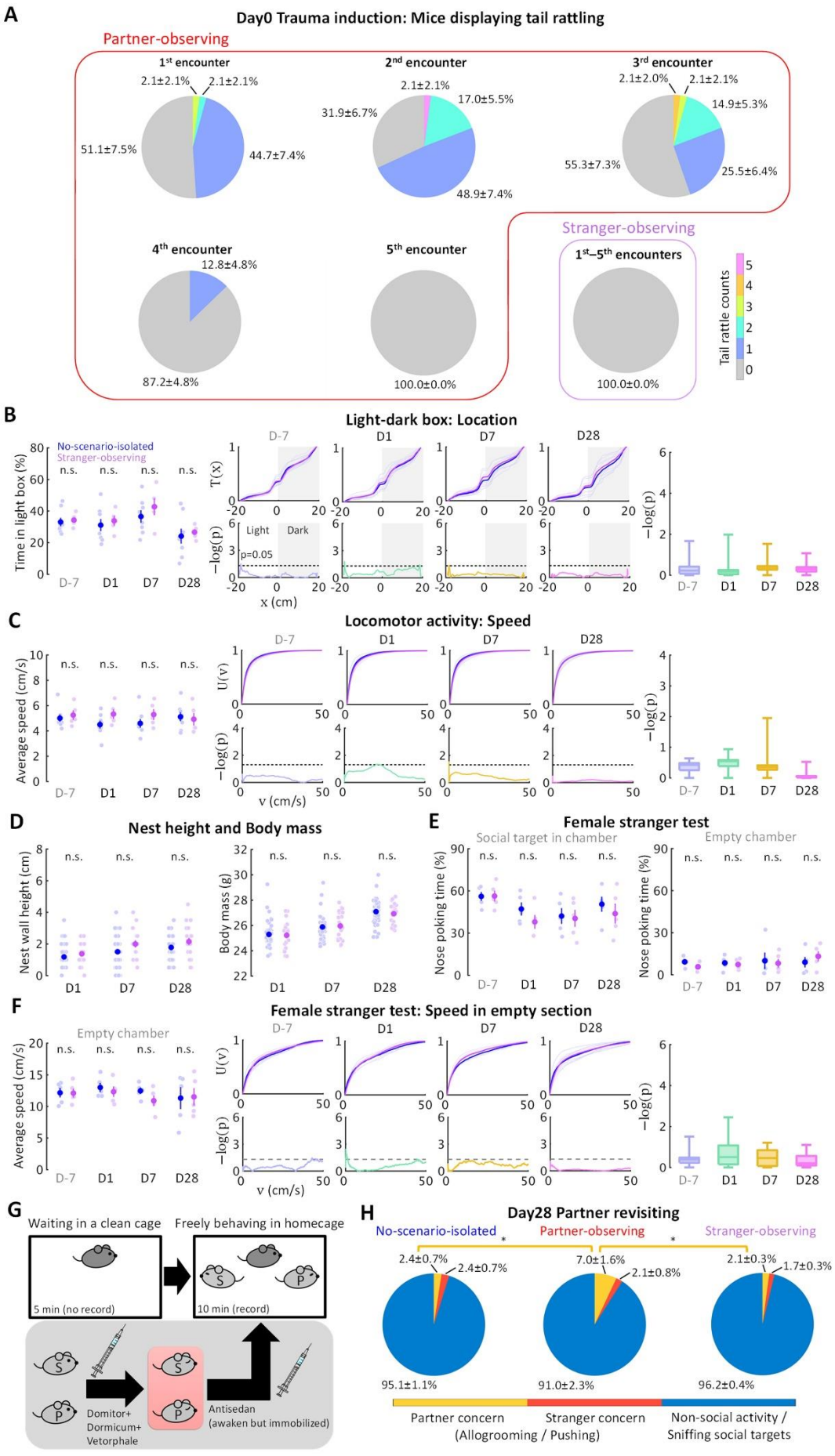
A
Day0 Trauma induction: Mice displaying tail rattling
Partner-observing
1st encounter
2.1±2.1%
2.1±2.1%
51.1±7.5%
44.7±7.4%
2nd encounter
2.1±2.1%
17.0±5.5%
31.9±6.7%
48.9±7.4%
3rd encounter
2.1±2.0%
2.1±2.1%
14.9±5.3%
55.3±7.3%
25.5±6.4%
4th encounter
12.8±4.8%
87.2±4.8%
5th encounter
100.0±0.0%
Stranger-observing
1st–5th encounters
100.0±0.0%
Tail rattle counts
B
Light-dark box: Location
No-scenario-isolated
Stranger-observing
Time in light box (%)
n.s.
D-7
D1
D7
D28
T(x)
Light
Dark
p=0.05
−log(p)
x (cm)
C
Locomotor activity: Speed
Average speed (cm/s)
U(v)
v (cm/s)
D
Nest height and Body mass
Nest wall height (cm)
Body mass (g)
E
Female stranger test
Social target in chamber
Empty chamber
Nose poking time (%)
F
Female stranger test: Speed in empty section
Empty chamber
G
Waiting in a clean cage
Freely behaving in homecage
5 min (no record)
10 min (record)
Domitor+
Dormicum+
Vetorphale
Antisedan
(awaken but immobilized)
H
Day28 Partner revisiting
No-scenario-isolated
Partner-observing
Stranger-observing
2.4±0.7%
2.4±0.7%
95.1±1.1%
7.0±1.6%
2.1±0.8%
91.0±2.3%
2.1±0.3%
1.7±0.3%
96.2±0.4%
Partner concern
(Allogrooming / Pushing)
Stranger concern
Non-social activity /
Sniffing social targets

Figure 2.9. Social relationship in trauma induction determines stress development. **(A)** Social relationship increased emotional impact, evidenced by tail rattling behavior during trauma induction. **(B–F)** No significant chronic difference was found in Stranger-observing mice. **(G)** The partner-revisiting test. A stranger mouse (light gray S) and the previously pair-housed partner (light gray P), both immobilized, were presented as social targets. Pink rectangle, heating pad. **(H)** Partner-observing mice showed significantly longer allogrooming or pushing their partners (yellow, % of time spent in partner concern behavior) than either No-scenario-isolated or Stranger-observing mice. Standard errors were calculated from bootstrapped data.

tail rattling during aggressive encounters and hiding under bedding material with the partner during resting were observed in 83% (n = 39 out of 47 mice) and all (n = 47 out of 47 mice) Traumatized mice, respectively, no such behaviors were shown by Stranger-observing mice (n = 0 out of 20 mice). In Traumatized mice, the frequency of tail rattles dropped progressively during aggressive encounters (Figure 2.9A), suggesting that it represents a rapid phasic psychological reaction during trauma induction. These results suggest that social relationship rapidly modulated emotional impact and social reactions during trauma induction. Moreover, chronic behavioral differences were not observed in Stranger-observing mice (Figure 2.9, B to F), which further excluded potential effects from salient, non-specific environmental manipulation (e.g. rotation through aggressors' homecages) and sensory shock (e.g. olfactory cues from urine and vocalization indicating fear) in trauma induction. To further characterize the effects of social relationship, I examined the impact of social support on behavioral developments by a fourth control group of mice (Buffered mice) as each of them was kept pair-housed with its attacked partner after trauma induction. Developments of the differences in emotionality of stress did not occur in Buffered mice (Figure 2.8, A to C), but developments that reflected their sociality showed the differences of Traumatized mice (Figure 2.8, D and E). Considering that social transfer of stress was elucidated in the early phase following an acute stress in mice (Sterley et al., 2018), my data demonstrate a role of social buffering that reduce the effects of stress incubation process observed during the late phase after an acute stress. The observation suggests that Buffered mice showed an emotional recovery from experiences of distress when being together with their partners, which further supports that emotionality and sociality during stress incubation were separately regulated. Taken together, the results of these control experiments reveal that social relationship constitutes a critical psychological factor that determined post-traumatic psychobehavioral development.

An important question remained: Why was stress incubated, but not attenuated? As traumatic consequences were modulated by social relationship, I hypothesized that

acute traumatic induction yielded chronic stress experience through partnership memory during social isolation, similar to human tending to recall relatively vivid memories of the past relationship after a traumatic relationship dissolution (Chung et al 2003). I examined the persistence of social memory in a partner-revisiting test on Day28 (Figure 2.10C; n = 5 mice for each group). Social stimuli were the previous partner and a stranger mouse, both immobilized to allow enough social cues to be attractive, but no active interaction with the focal mouse. To avoid possible influences of social cues from socially defeated mice, stranger mice used to test Control and Stranger-observing mice were partners of Traumatized mice. Strikingly, Traumatized mice spent three times as much time allogrooming or pushing their previous partners as did Control and Stranger-observing mice (Figure 2.9D). This amount of allogrooming or pushing previous partners is similar in Buffered mice which were kept pair-housed with their attacked partners until the partner-revisiting test (Figure 2.9E). The preference of Traumatized mice to their previous partners, together with the findings of chronic anxiety (Figures 2.3 to 2.6) and social apathy (Figure 2.7) after separation, suggests affectional bonding as a key mechanism of stress incubation in this paradigm (Figure 2.10).

2.4 Discussion

I present a novel approach to interpret previously challenging and inconclusive behavioral development, centered on the study of PTSD-like internal psychological development in laboratory mice. These results demonstrate the first system-level view of experimentally disentangled components, processes, and determinants in post-traumatic stress development. While my data suggest that laboratory mice and PTSD patients share similar post-traumatic reactions and psychological substrate, I found little support for the common view that a complex association among trauma-induced

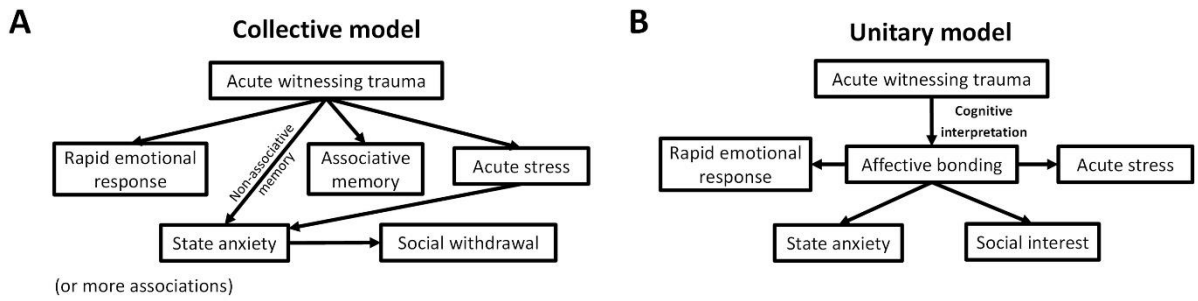

Figure 2.10 Conceptual models explain PTSD development. Foregoing data demonstrate a unitary psychopathological model with its corresponding neural substrate for the stress development paradigm in this study. My data show little support for a collective view speculated in previous hypotheses **(A)**, but support a unitary view **(B)** where diverse PTSD-like reactions independently developed via a common cognitive source ("Affective bonding"). This unitary view suggests a psychological substrate in system-level that integrates multiple mechanisms underlying highly diverse behavioral consequences, as a specific clinical target in the full mechanistic picture.

psychological states govern the developmental process (Bryant et al 2017, DSM-5 2013, DSM-III 1980, Ehlers & Clark 2000, Hayes et al 2012, Pamplona et al 2011, Schnyder & Cloitre , Siegmund & Wotjak 2006, Zoladz & Diamond 2013) (Figure 2.10). Instead, I propose a unitary view where the alternation of a single cognitive source is sufficient for triggering changes of diverse and rather independent psychological states. Accordingly, I expect that behavioral signs of PTSD development could also be detected in humans already shortly after the traumatic event, which are likely to be independent of acute stress reactions. The fine-scale behavioral analyses introduced here provide a simple, non-invasive analytic tool to capture informative behavioral details and are not limited to laboratory animals, opening a new window for early detection and prediction to prevent a development into PTSD.

Importantly, although multiple other interpretations have been ruled out by cross-testing and cross-experimenting comparisons, my observations could have alternative explanations. For example, the observation that Partner-observing mice interacted more with their former cagemates could reflect a memory reduction that they felt their former cagemates were more novel and therefore worth-exploring. However, while this may be the case reflecting a false memory, the observed difference did support a memory, which was affected by trauma according to cross-experiment comparisons. In addition, the false memory is less likely to explain the observations in Partner-observing mice, as they behaved similarly to Partner-buffered mice with which their partners were pair-housed until the partner-revisiting test. Accordingly, Partner-observing mice were more likely to represent their memory of social bonding. As another example, since my data did not replicate common findings of social avoidance followed by social defeat stress at both early and late testing time points, a dose responses of observational stress could govern this "micro-defeat" which did not result in a full standard constellation of PTSD-like behaviors in mice, so that Partner-observing mice may reflect their weak social avoidance to the novel targets compared with a safe and familiar one. Nevertheless, because Partner-observing mice kept

spending more or similar time in nose poking compared with their behaviors during the non-social session, a social avoidance is less likely to account for these observations, which is more likely to consider as a reduction of social interest that reflects an apathy-like reaction. Finally, while researches on animal emotion usually focus on their ability to show human behavioral and physiological conditions (face validity), to reproduce pharmacological effects in human (predictive validity), and to share the same biological processes as human (construct validity), a few studies have taken the possibility of human-unique, animal-unique, and human-animal-sharing emotions under a consideration. In my study, I demonstrated a putative human-animal-sharing emotion by starting from a complete, exclusive, and non-human-unique definition of the focused emotional feature and logically evaluating both explanatory and predictive power of the inferences driven from which but not the other way around. Thus, I concluded that the most parsimonious interpretation of the overall observed phanamana in the present study is that mice had various classes of negative responses to observed trauma which were rather independent and determined by a single common factor.

While much remains to be considered before clinical applications, including a corresponding study in humans, my study establishes a solid basis to uncover psychological theories for therapeutic strategies (Schnyder & Cloitre). More than leading toward a better efficacy and lower risk in conducting psychological treatments, this foundation provides a platform to test the role of biological substrates in a system-level view that integrates multiple mechanisms underlying highly diverse behavioral consequences (Figure 2.10). For instance, a path toward brain physiology can be to test how the potentially slow and global change of brain dynamics arises from an altered dynamic in social bonding circuits through their interconnected nodes (Amadei et al 2017, Funamizu et al 2016a, Ko 2017, Lee et al 2015, Lee et al 2014). The efficacy of pharmacotherapies could therefore be improved. Beyond PTSD, my research approach to imply human complex psychology by quantitatively and

experimentally inferring intertwined psychological qualities in laboratory mice opens a wide range of possibilities in psychiatry.

2.5 Summary and conclusion

Despite a broad research focus on the diverse symptoms of post-traumatic stress disorder (PTSD), the gradual emergence of symptoms following trauma exposure remains as a major conceptual challenge. I identified and examined behavioral development in mice isolated after observing a traumatic event inflicted upon their pair-housed partners. Compared to mice isolated without traumatic experience, fine-scale behavioral analysis showed that anxiety-related reactions gradually increased through isolation, while the early phases were independent of acute stress reactions. Instead of social avoidance, traumatized mice presented long-term social apathy to strangers. These behaviors were not observed if the traumatic event happened to strangers. Additionally, traumatized mice showed rebound responses to their partners after a long separation. Concluding, a single common factor, affectional bonding, underlies the rather independent development of PTSD-like behaviors in mice. The observed psychological homology between mice and humans emphasizes the potential of rodent models to untangle subtle psychobehavioral development in humans.

3 Toward neuronal dynamic framework for spontaneous behaviors

3.1 Introduction

A detailed understanding of the relation between observed dynamics and underlying computation is critical to explain how the brain computes lie embedded in the complexity of neuronal circuit responses for diverse behaviors. Outside from any behavioral task, awake animals irregularly initiate, keep, and suspend various behaviors in a homogenous and steady environment (Bartumeus 2009, Bazazi et al 2012, Brembs 2011). Spontaneous behaviors of a single animal in a steady environment has been taken as a fundamental representation of internal states such as emotion (Lee et al 2018). During free social interactions, behaviors of social and non-social reactions also alter irregularly (Hoopfer et al 2015, Remedios et al 2017). Complex dynamics of spontaneous behaviors show structured patterns and do not reflect random noise from environmental fluctuations (Benhamou 2014, Maye et al 2007, Proekt et al 2012). These irregular but structured patterns are therefore believed to represent the underlying background brain activity and its dynamics (Benhamou 2014, Censi et al 2013, da Silva et al 2018, Dipoppa et al 2018, Rosner & Warzecha 2011, Stringer et al 2018). While models of neuronal dynamics for behavior initiation have been well developed to explain goal-guided actions [e.g. (Funamizu et al 2016b, Mante et al 2013)], these models have been challenged to explain animal spontaneous behaviors. To date, neuronal dynamics for generating, maintaining, and terminating spontaneous behaviors remain mysterious.

Neuronal command activities that showed specificity to the type of movement were found to be preceded by preparatory discharges of readiness neurons that showed less specificity, which were further shown to be shaped by their sequential excitatory and inhibitory synaptic inputs from local circuits [e.g. supraesophageal ganglion neurons of crayfishes (Kagaya & Takahata 2011)]. Also, it was shown for several subcortical brain regions in laboratory rodents that their neuronal activities is

necessary for spontaneous movement initiation [e.g. dopamine neurons of the substantia nigra pars compacta for locomotion (da Silva et al 2018)], movement repertoire [e.g. estrogen receptor-α expressed neurons of the ventrolateral subdivision of ventromedial hypothalamus for aggression (Hashikawa et al 2017, Lin et al 2011)], and movement termination [e.g. striatal medium spiny neurons for action sequences (Jin & Costa 2010)]. These activities for voluntary actions were suggested to be regulated by cortical influences (Kawai et al 2015) that support the physical substrate of consciousness (Tononi et al 2016). Ongoing cortical activity has been proposed to be a consequence of functionless network chaos even impairing cortical representations (Parga & Abbott 2007, Stringer et al 2016), a recapitulation of cortical memory and predictions (Berkes et al 2011, Luczak et al 2009), or a reflection of physiological and mental states (Gentet et al 2010, Niell & Stryker 2010). As an indication from behavioral uncertainty in goal-guided tasks, trajectory events of hippocampal place-cell sequences were found to roughly depict the future paths of rats (Pfeiffer & Foster 2013). Moreover, self-initiated giving up of waiting a reward was demonstrated to be determined by the ramp-to-threshold activity of integrator neurons in the secondary motor cortex through summing up their inputs (Murakami et al 2014). However, these studies on neural mechanism underlying spontaneous or uncertainly voluntary behaviors were mainly limited in two logical approaches: (i) to identify a premotor activation with an investigation of its regulatory influences, and (ii) to analyze collective properties of neural and behavioral dynamics with an investigation of their regulatory factors. Therefore, a control mechanism explaining both temporally fine-scaled and global observations remains unclear. By combining two-photon calcium imaging in head-restrained mice with a prediction-based investigation of neuronal population dynamics for the generation, maintenance, and termination of spontaneous behaviors, here I developed a novel research approach to achieve implications about the control mechanism explaining the temporal organization of spontaneous neuronal dynamics and spontaneous behaviors.

3.2 Methods

All animal experiments were approved by the Institutional Animal Care and Use Committee (IACUC) in the animal facility at the Okinawa Institute of Science and Technology (OIST) Graduate University, accredited by the Association for Assessment and Accreditation of Laboratory Animal Care (AAALAC).

3.2.1 Study design

Sample size. No statistical methods were used to predetermine sample sizes. Animal numbers were determined based on previous studies.

Rules for stopping data collection. Mice after the surgery were expected to be in a risk of adverse events that lead to a loss of body weight, abnormal behaviors, severe bleeding, or contaminated wound exposure. Mice that were found with severe bleeding or contaminated wound exposure were euthanized. After survival surgery, the mouse was weighed every day for up to 1 week following surgery. If the body weight decreased by 20% or more, or the mouse showed ataxic, stereotypic, or dysfunctional behaviors, the first immediate measure was to check the dehydration by testing the skin elasticity with a light pinch. If the animal is dehydrated, saline was injected subcutaneously. The second measure was to check the inflammation by observing characteristic signs of redness, swelling, and heat. If the area around the implant appeared inflamed, additional anti-inflammatory analgesic was given. If these treatments were effective but the abnormal signs tested by these measures still remained on the next day, the mouse was treated again as previously described, while these measures and treatments were repeated daily the until the mouse got normal. If none of these measures and treatments was effective, the mouse was euthanized.

Data inclusion/exclusion criteria. No data was excluded.

Outliers. No outliers were defined.

Selection of endpoints. The endpoints were prospectively selected.

Replicates. All data collections were conducted in double to triple sampling replicates, each conducted in a single experimental cohort.

Research objectives. The goal of this work is to identify a dynamic framework of subcellular activities across cortical subnetworks and their laminar architectures for generating, maintaining, and terminating spontaneous behaviors in laboratory mice. Pre-specified hypotheses stated that (i) distinctive network components (areas and layers) of the cerebral cortex are captured in the dynamic but not the stative features of a few leading population-level patterns, and (ii) continuously ongoing neuronal patterns are better explained by a closed-loop control system (control action from cortical activities, as in the process of a controller, are dependent on feedback from behaviors, as the process output) than by an open-loop control system (control action from cortical activities are independent of behaviors), while (iii) the knowledge of (i) and (ii) allows to explain and predict dynamical features and the initiations of animal spontaneous behaviors. All other hypotheses were suggested after initiation of the data analyses.

Research subjects or units of investigation. 8-week-old male C57BL/6J mice were used.

Experimental design. I approached the research goal by investigating neuronal population activities in layers 1, 2, 3, and 5 of the primary somatosensory cortex (SI), posterior parietal cortex (PPC), anterior cingulate cortex (ACC), primary motor cortex (MI) by two-photon calcium imaging in head-restrained mice during spontaneous behaviors (Figure 3.1). To solve previously inaccessible problems in tong-term recording and signal extraction, technical developments for processing neuronal and behavioral data were introduced and validated. The investigating analyses included statistical methods for quantifications of collective properties, dimensional reduction, characterization of dynamical structures, predicting tests by artificial neural networks, control system modeling. The control analyses included statistical comparison with

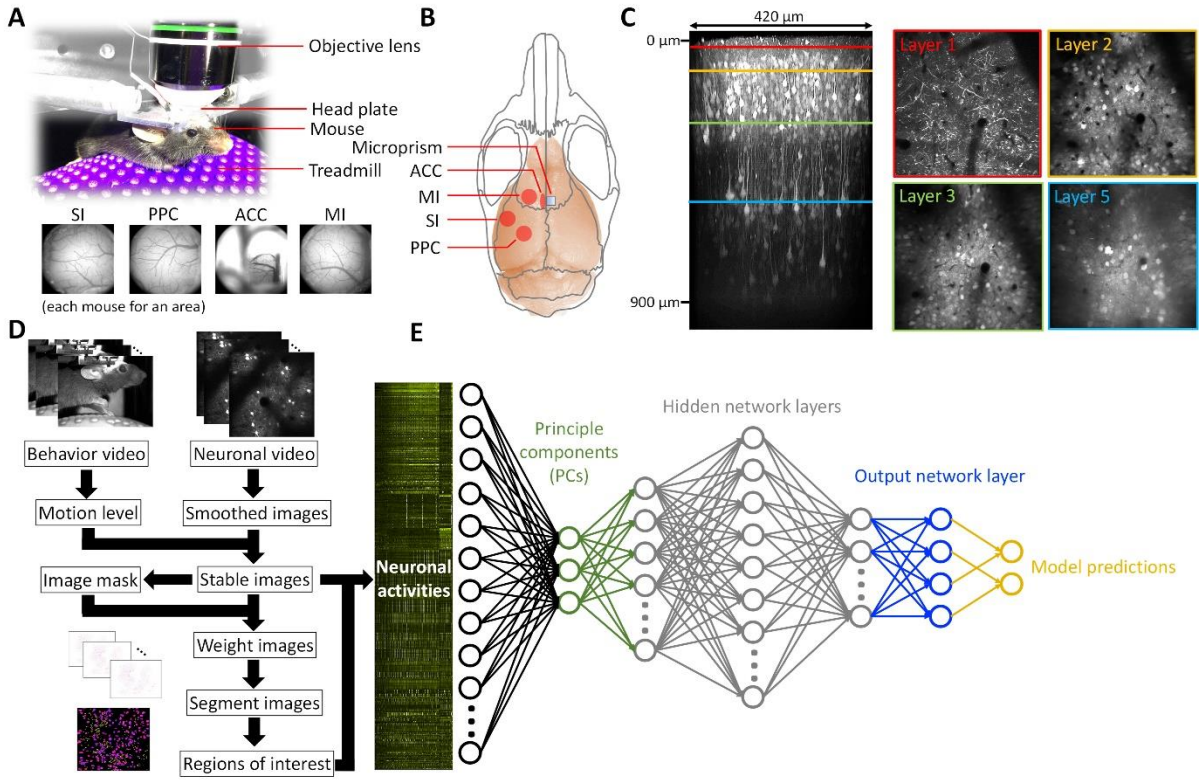

Figure 3.1. Experimental paradigm and automatic data processing without arbitrarily assigned parameters. **(A)** Experimental setups of two-photon calcium imaging in head-restrained mice. **(B)** Schematic illustration of the 4 focal cortical areas chosen in this study: the primary somatosensory cortex (SI), posterior parietal cortex (PPC), anterior cingulate cortex (ACC), and primary motor cortex (MI). **(C)** Z-stack TurboRFP image and GCaMP6f frame-scanned images illustrate the 4 focal cortical layers (layers 1, 2, 3, and 5) in this study. **(D)** Schematic algorithm of automatic behavioral and neural data processing. **(E)** Neural network diagram demonstrates data-based prediction approach. In particular, model predictions that was based on the neural activity in this study are the future behavioral motion levels, to demonstrate the control principles of neurobehavioral association during spontaneous behaviors.

the results from effectors of potential systematic errors, data sets created by data bootstrapping and data shuffling, and model generating data.

Randomization. Mice were from different litters. Mice were randomly allocated into an experimental group for one of the four recorded brain areas.

Blinding. The investigator was not blinded to the group allocation during data collection and/or analysis.

3.2.2 Overview

In total, 12 male C57BL/6J mice (CLEA Japan, Inc.) were used in this study, with 3 mice for each of the 4 recorded cortical areas. Before the experiments, mice were group-housed (≤5 mice per cage) in 380×180×160-mm transparent holding cages (Sealsafe Plus Mouse DGM - Digital Ready IVC; Tecniplast Inc., Quebec, Canada) bedded with 100% pulp (FUJ9298101; Oriental Yeast Co., Ltd., Tokyo, Japan) under a 12-hr dark/light cycle (350-lux white light) at a controlled temperature of 22.7 – 22.9 ˚C, humidity of 51 – 53%, and differential pressure of -14 – -8 Pa with food and water available *ad libitum*. After surgeries of chronic window preparation, mice were housed individually, provided with a pair of InnoDome™ and InnoWheel™ (Bio-Serv, Inc., Flemington, NJ, USA), under a 12-hr dark/light cycle (350-lux white light) at a controlled temperature of 22.7℃, humidity of 53 – 55%, and pressure difference of -57 – -34 Pa with food and water available *ad libitum*. Circadian time (CT) is defined to start at mid-light period and described in a 24-hr format, i.e. light off at CT 6:00.

The experimenter and caretakers wore laboratory jumpsuits, lab boots, latex gloves, face masks, and hair nets when handling mice and performing experiments. All behavioral training and imaging experiments were conducted during the dark cycle (CT 6:00–11:00). Handling of mice during the dark cycle was done under dim red light and mice were transported in a lightproof carrier within the animal facility.

3.2.3 Surgical procedures

Surgeries were performed in a surgery room with controlled temperature of 22.4 – 23.0 °C, humidity of 54 – 55%, and pressure difference of -9 – -4 Pa in the animal facility. Mice were initially sedated with 3% v/v isoflurane in oxygen and subsequently kept anesthetized with 1% v/v isoflurane in air, followed by injections of saline (1,000 μl; 0.9% NaCl; *s.c.* to the back), dexamethasone sodium phosphate [2 μl/g (body weight) of 2 mg/ml in 0.9% NaCl; *i.m.* to the left femoris muscle], rimadyl (10 μl/g of 1 mg/ml in 0.9% NaCl; *i.p.* to the left abdomen), and mannitol [10 μl/g of 150 mg/ml in phosphate-buffered saline (PBS); *i.p.* to the left abdomen]. Eye ointment (Sato Pharmaceutical Co., Ltd., Tokyo, Japan) was applied to the eyes and body temperature was maintained at 36.5° C with heating pad. The heads of the mice were immobilized in a stereotactic frame by blend ear bars and a nose cone. After the fur was shaved and removed with hair removal cream (Veet Hair Removal Cream – Sensitive Skin; Reckitt Benckiser Group plc., Slough, UK), the epicranium was removed to expose the skull over the left or both hemispheres. The skull was cleaned with dilute iodine tincture (KENEI Pharmaceutical Co.,Ltd., Osaka, Japan) and 2% lidocaine solution (20mg/ml; Maruishi Pharmaceutical Co., Ltd., Japan).

A circular craniotomy (4.0 mm of diameter) was made without puncturing the dura mater (Roome & Kuhn 2014) over the primary somatosensory cortex (SI; centered at 1.0 mm posterior and 3.0 mm left of the bregma), posterior parietal cortex (PPC; centered at 2.0 mm posterior and 2.0 mm left of the bregma), primary motor cortex (MI: centered at 1.0 mm anterior and 1.0 mm left of the bregma), or anterior cingulate cortex (ACC; centered at 1.0 mm posterior and 0.0 mm left of the bregma) (Figure 3.1B). Fixation of the head in the stereotaxic instrument was adjusted so that the virus injections and chronic window preparation were made perpendicularly to the brain surface (0° around yaw, 0° around roll, and +20° around pitch for SI; 0° around yaw, 5° around roll, and -10° around pitch for PPC; 0° around yaw, 0° around roll, and 0° around pitch for ACC and MI).

A 1:1 mixture of the viral vectors AAV2/1-SYN-GCaMP6f [2×10^{13} genomic copies (GC)/ml; Penn Vector Core, PA, USA] (Chen et al 2013b) and AAV2/1-SYN-TurboRFP (3×10^{13} GC/ml; Penn Vector Core, PA, USA) were prepared for labeling neurons. For mice prepared for imaging SI, PPC, or MI, 6 injections of the mixture (35 nl per injection over 8 minutes, left at each place for 3 minutes before and after each injection) were performed at 3 positions (roughly a regular triangle with 300 μm of side lengths) each with 2 depths (the first at 400 μm and the second at 800 μm beneath the surface of the dura), centering at 800 μm posterior and 3,000 μm left to bregma for SI, 1,800 μm posterior and 1,700 μm left to bregma for PPC, and 800 μm anterior and 1,400 μm left to bregma for MI. For mice prepared for imaging ACC, 3 injections of the mixture (70 nl per injection over 15 minutes, left at each place for 5 minutes before and after each injection) were performed at 3 positions (400 μm, 700 μm, and 1,000 μm anterior and 400 μm left to bregma) each with 1 depth (1,000 μm beneath the surface of the dura). All injections were made using beveled quartz pipettes (tip with outer diameter of 22.5 – 30.0 μm and inner diameter of 10.0 – 15.0 μm), a custom air pressure injection system, and a micromanipulator (MP-285; Sutter Instrument Company, CA, USA).

After the injections, for mice prepared for imaging SI, PPC, and MI, a glass window (5-mm diameter, 170-μm thickness) was mounted directly on the dura of the 4-mm craniotomy and sealed to the skull with super glue. For mice prepared for imaging ACC, a 1.5 mm×1.5 mm durotomy was made along the right edge of superior sagittal sinus 0–1.5 mm anterior to bregma on the right hemisphere, and the same glass window but attached with a 1.5 mm × 1.5 mm microprism was inserted into the longitudinal fissure (Low et al 2014) and mounted on the craniotomy with the skull sealed with super glue. An aluminum head plate was then attached to the skull with dental acrylic (Super-Bond C&B; Sun Medical, Shiga, Japan). At the end of the surgery, 5% lidocaine cream (25 mg/g of lidocaine and 25 mg/g of prilocaine; EMLA Cream 5%, AstraZeneca plc.; Sato Pharmaceutical Co., Ltd.) was applied to the epicranium, followed by the injection of 2.5 μl/g buprenorphine (0.2 mg/ml in 0.9% NaCl; *s.c.* to the back). The mouse was kept on a heating pad at 34°C (B00O5X4LQ2; GEX Co., Ltd.,

Osaka, Japan) to maintain their body temperatures before it awaked from the anesthesia. The mass of entire implanted device was about 600 mg.

3.2.4 Behavioral training

All behavior training was performed under dim red lights or the dark in the behavior training room with controlled temperature of 22.5 – 23.1 °C , humidity of 53–56% , and pressure difference of -5 – -2 Pa. On the 8th day after surgery, the mouse was brought with its home cage to the behavior training room. The mouse was first tamed by a handler, allowing the mouse to freely move between the arms for 10 min. The mouse was then transferred to a styrofoam cylinder (14 cm in diameter) and allowed to move on it without restraint for another 10 min, with the handler rotating the cylinder to keep the mouse near the top. After the training, the mouse was returned to its homecage and brought back to the holding room.

On the 10th day after surgery, the second training section was started with unrestrained moving on a styrofoam cylinder for 10 min as previously described. The mouse was then placed and head-fixed on the cylinder treadmill setup and allowed to behave freely for 30 min. After the training, the mouse was returned to its homecage and brought back to the holding room.

On the 12th, 14th, 16th, 18th, and 20th day after surgery, the training began with head-restrainedly behaving on the spherical treadmill for 1 hr, 2 hr, 3 hr, 3 hr, and 3 hr, respectively. After the training, the mouse was returned to its homecage and brought back to the holding room.

3.2.5 Two-photon imaging with behavior recording

Imaging was performed with a custom-built combined wide-field and two-photon microscope [Movable Objective Microscope (MOM); Sutter Instrument Company, CA, USA] (Figure 3.1A). A 5x/N.A. 0.25 air objective (Carl Zeiss AG, Jena, Germany) was used to image the blood vessel pattern of the cortical surface in wide field. For long-term two-photon recording, ultrasound gel (Clear Image; Sonotech, TX,

USA), instead of dH_2O, was applied to a 25x/N.A. 1.05/Collar 0.17 water immersion objective with 2 mm working distance (Olympus, Tokyo, Japan) for experiments imaging SI, PPC, and MI, or to a 25x/N.A. 1.00/Collar 0.17 water immersion objective with 4 mm working distance (Olympus, Tokyo, Japan) for experiments imaging ACC. A femtosecond-pulsed Ti:sapphire laser (Vision II; Coherent, CA, USA) was used to excite the fluorophore. Fluorescence was split with a dichroic mirror (565DCXR; Chroma Technology Corporation, VT, USA) and selectively band-pass filtered with a 605±35 nm filter (ET605/70m-2P; Chroma Technology Corp, VT, USA) and a 525±35 nm filter (ET525/70m-2P; Chroma Technology Corp, VT, USA) for TurboRFP and GCaMP6f, respectively. Fluorescence was detected with two GaAsP photomultiplier tubes (Hamamatsu Photonics K.K., Hamamatsu, Japan). The microscope and image acquisition were controlled by commercial software MScan (Sutter Instrument Company, Novato, CA, USA).

On the 21th day after surgery, the mouse was brought with its home cage to the imaging room with controlled temperature of 22.1 – 23.3°C and humidity of 45 – 56%. The mouse was then placed and head-fixed on a cylinder treadmill in a Faraday cage of the microscope setup in complete darkness. To determine the surface of the brain, the Ti:sapphire excitation laser was operated at 1000 nm for observing the second harmonic signal of dura collagen. The laser was then adjusted to 955 nm for neural imaging, with laser power up to 80 mW at the back focal plane for layer 5 imaging, 1 – 5 mW power at the focus. Images were acquired at 30.9 Hz by a resonant scanning system at a resolution of 512 × 512 pixels (420 × 420 μm field-of-view). Cortical layers were identified based on the laminar organization of cellular histology (Figure 3.1C): Layer 1 was identified as the depth around the center between the deepest end of dura and the surface of upper pyramidal layer where the density of fluorescence-expressed somata dramatically increased (64–81 μm, 59–83 μm, 58–70 μm, and 54–71 μm beneath the deepest end of the dura for SI, PPC, ACC, and MI, respectively); Layer 2 was identified as the surface part of upper pyramidal layer where the density of fluorescence-expressed somata began to increase dramatically (150–170 μm, 147–160

μm, 128–175 μm, and 144–184 μm beneath the deepest end of the dura for SI, PPC, ACC, and MI, respectively); Layer 3 was identified as the deep end of upper pyramidal layer before the density of fluorescence-expressed somata began to decrease dramatically or before the density of fluorescence-expressed somata began to increase dramatically again with a larger size of somata (277–330 μm, 245–255 μm, 211–243 μm, and 233–247 μm beneath the deepest end of the dura for SI, PPC, ACC, and MI, respectively); Layer 5 was identified as the surface part of lower pyramidal layer where the density of fluorescence-expressed somata began to increase dramatically again with a larger size of somata (540–620 μm, 528–545 μm, 408–411 μm, and 358–397 μm beneath the deepest end of the dura for SI, PPC, ACC, and MI, respectively). The cortical layers were imaged straight downward from layer 1 ,2, 3, to 5 in order. During the 30-min recording for each layer, 56,000 frames were recorded.

Spontaneous behavior was simultaneously video-taped during brain imaging at the same sampling rate with a video camera (640 × 480 pixels; FireDragon CCD, Behavior Video, Sutter) from the right side of the mouse, with two additional frames of one before and one after neural imaging records. In addition, the treadmill rotating speed was detected using a rotary encoder (360 pulse/rotation; E6A2-CW3C; Omron Corporation, Kyoto, Japan) and recorded in 1,000-Hz analog traces of two square waves in quadrature. After recording, the mouse was anesthetized with 1% v/v isoflurane in air on the setup. Z-stack images of the cerebral cortex between 0 – 1,000 μm beneath the surface of the dura were then made with 1 μm Z-intervals.

3.2.6 Histological procedures

After the imaging experiments, mice were deeply anaesthetized with a ketamine-xylazine mixture (>30 μl/g body weight of 100 mg/ml ketamine and 20 mg/ml xylazine) and perfused transcardially. The perfusates, in a three-step procedure, were (i) 20 ml of ice cold 1x phosphate-buffered saline (PBS), (ii) 20 ml of ice cold 4% paraformaldehyde, 0.2% sodium meta-periodate, and 1.4% lysine in PBS, and (iii) 20 ml of ice cold 1x PBS. After perfusion, the brain was carefully removed from the

cranial bone and store in ice cold 1x PBS. Coronal sections of the forebrain were sectioned into 100-μm slices with a vibratome (VT1000S; Leica Camera AG, Wetzlar, Germany). Recording sites were examined with a macro confocal imaging system (C2si-Az100; Nikon Corporation, Tokyo, Japan).

3.2.7 Data process

Raw data of two-photon imaging with behavior recording were processed using custom scripts written in MATLAB R2014b (MathWorks) with a desktop computer (40-core 2.30 GHz Intel Xeon Processor E5-2698 v3, Hynix Original 512GB LRDIMM Server Memory Upgrade for Server DDR4 2400MHz RAM Memory Kits; Dell Precision T7910 Tower Workstation; Dell Inc., Round Rock, TX, USA). All acquisition parameters, neural imaging records, behavioral video records, and analog signal records from a 30-min recording were stored as MCS (mathcad image) data files and packaged in a single MDF (measure data format) file. MCS data files were opened and read using the OpenMCSFile method through MCSX (MView; Sutter Instrument Company) instantiated by MATLAB. All data sets were processed fully automatically without any parameter assignment through the following algorism (Figure 3.1D).

Analog traces of recording treadmill rotation and resonant scanning were read as 16-bit signed integers. After the square waves recording treadmill rotation were binarized, both movement direction and the count indicating distance traveled were decoded. By referring the trace of triangle wave recording resonant scanning for neural images, speed and velocity of mouse locomotion on the treadmill were then calculated when reducing the sampling rate from 1,000 Hz to 30.9 Hz in alignment with neural imaging and behavior video frames.

Video frames of behavior recording were read as a 2-dimensional matrix with an 8-bit gray scale. Motion energies was calculated as the averages of absolute values of subtractions of corresponding pixels between temporally adjacent frames. Motion levels were taken as the absolute values of subtractions between temporally adjacent motion energies. Motion states of resting and moving were binarized according to the

threshold defended as the second value where the counts in the distribution of motion levels with 1,000 bins stopped decreasing from the peak count (Figure 3.2A).

Imaging frames of neural recording were read as a 2-dimensional matrix with a 16-bit gray scale. By referring the binary trace of motion states, TurboRFP imaging frames recorded during the longest resting period were averaged into a template image. All TurboRFP and GCaMP6f imaging frames were then aligned according to fast normalized 2-D cross-correlation (Yoo & Han 2009) referring the template image.

To sort out regions of interest (ROIs), a mask image was obtained from a five-step calculation: (i) getting normalized frames, each taken as a GCaMP6f imaging frame divided by the average of all GCaMP6f imaging frames, (ii) getting normalized rate frames, each calculated by subtracting temporally adjacent normalized frames, (iii) computing rate absolute values, each of a normalized rate frame divided by three powers of the standard deviation of the full normalized rate frames, (iv) computing the threshold, as one seventh of the maximum of the rate absolute values, and (v) binarization according to the threshold, to mask out pixels which had no absolute values in the time trace above the threshold. After GCaMP6f imaging frames were reduced 10 times of the sampling rate by taking the maximal value in a time window, the mask image was applied to each rate-reduced GCaMP6f imaging frames. The first fifty PCA (principle component analysis) eigen-images were obtained from PCA on the rate-reduced GCaMP6f imaging frames (Halko et al 2011). Twenty ICA (independent component analysis) eigen-images were then obtained from ICA on these fifty PCA eigen-images. Normalized weight images were calculated by spatial z-scores with respect to the mean and standard deviation of each weight image obtained by taking the absolute values of each ICA eigen-image. Segment images were then taken by binarizing the normalized weight images at the threshold of 1.96. ROIs were sorted out from all segment images by removing segments with sizes <9 pixels and those had >20% of their sizes overlapped with other segments.

Raw signal traces were taken as the averaged signals within the ROIs through each GCaMP6f imaging frame. Signal traces were normalized by calculating $\Delta F/F$

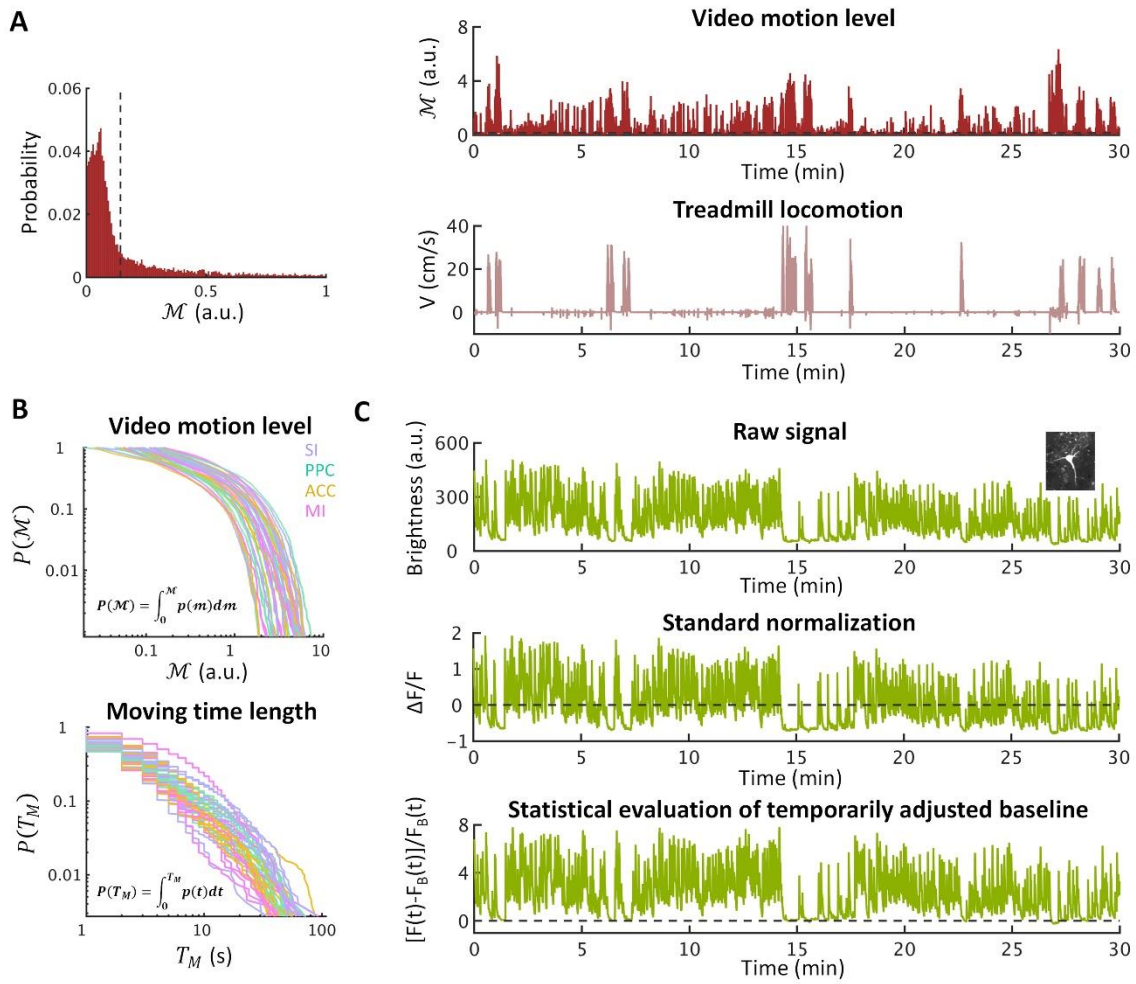

Figure 3.2. Validation of data process reveals a more reliable data representation than previous methods. **(A)** A comparison between quantitative behavioral traits from video recording (upper-right panel) and treadmill rotation (bottom-right panel) display behavioral diversity of head-restrained mice. Binarily distinctive behavioral states of stationary (i.e. resting) and moving periods were determined according to the threshold statistically determined by the distribution of motion levels quantified from video recording ($\mathcal{M}$) (left panel). **(B)** Validation of individual and trial variance of spontaneous behaviors by the reverse cumulative probability distributions (P) of movement aptitudes ($\mathcal{M}$; upper panel) and moving periods (T_M; bottom panel) plotted with double logarithmic scales to represent stochastic structures of the data. The results showed no difference among mice with different recorded cortical areas. **(C)** Calcium activity (upper panel) of a highly active neuron (inserted image) emphasizes a more reliable method of signal normalization reported in this study (bottom panel) than the standard method (middle panel).

where the baseline for each time point was determined by the signal aptitude with the peak count in the distribution of raw signals with 1,000 bins in the ±2.5-min time window with respect to each time point (Figure 3.2C). For signals within the first and last 2.5 min, the first and last 5-min time window were referred, respectively. Baseline value was updated only if it became lower. To reduce the effect of decay time constant of calcium signal to spiking activity, both regarding to the data sampling rate and a more reliable signal representation, neuronal calcium activities for these analyses are now based on their changing rates, while only significantly increased activities (z-scores greater than 2.33) were counted in.

3.2.8 Artificial neural network

To test the causal association between neural activity and behavioral motion level, predictability that reflects causal inferences was measured by the accuracy of future motion level predicted by current neural activity (Figure 3.1E), and *vice versa*. Artificial neural networks were created and trained with custom scripts written in MATLAB R2014b (MathWorks). Network architecture for all predictions was selected as a deterministic 3-layer feedforward network with hidden layer sizes of 12, 15, and 10 units, respectively, using log-sigmoid transfer functions. Each network was trained by using Levenberg–Marquardt algorithm, with a random data division of 80% for training and 20% for testing. Training of updating weights and biases was stopped when reaching 1,000 iterations, obtaining a perfect data fitting [the mean squared error (MSE) equaled to zero], having the error rate continuously increasing for more than 6 epochs, showing the gradient of MSE less than 10^{-7}, or receiving the training gain larger than 10^{10}. The predictability was evaluated by calculating the inversed values of MSEs compared with the data set used for testing and -log(p) of the p-value from comparing the means of MSEs from data and those from shuffled data that motion level sequence was temporally shifted.

3.2.9 Statistical analysis

Numerical data were analyzed with custom scripts written in MATLAB R2014b (MathWorks). Statistical significance of the difference between 2 mean values was

estimated with two-tailed, two-sample Student's *t*-test. Temporal cross-correlation was represented in the coefficient of determinations (r^2, where r is the Pearson correlation coefficient) with positive time lags for delaying the referred trace and negative time lags for proceeding the referred trace. PCA was computed using the covariance method and each orientation to a PCA axis is assigned so that the difference between maximal and mean values are larger than that between minimal and mean values. ICA was computed using FastICA algorism with Gaussian negentropy. Network predictivity was taken as the inverse of mean squared error (MSE). Standard errors of means for results across animals were estimated with the formula $\sigma/\sqrt{n}$, where σ is the sample standard deviation and n is the sample size.

3.3 Results

3.3.1 Region-specified features of neuronal population calcium activity

In the cerebral cortex [e.g. the primary somatosensory (Peron et al 2015), primary motor (Chen et al 2013a), posterior partial (Driscoll et al 2017), and anterior lateral motor (Li et al 2016) cortices in mice], neuronal calcium activities show a gradient of mixed encoding, including a majority of task-unrelated neurons. These divergent representations were reported to be a general feature of neuronal dynamics in various forebrain areas during spontaneous behaviors (Stringer et al 2018). According to subnetwork clusters organized through the intracortical connections (Zingg et al 2014), I focused on four cortical areas: the primary somatosensory (SI) and primary motor (MI) cortices of the somatic sensorimotor subnetwork which allows direct interactions between sensory (e.g. SI) and motor (e.g. MI) areas in the absence of higher-order association, and the posterior partial (PPC) and anterior cingulate (ACC) cortices of the medial subnetwork which mediates interactions between multiple sensory areas (e.g. PPC) and higher-order association areas (e.g. ACC). In addition, neocortical columns were demonstrated to contain two separate processing systems: layers 2/3 and 4 of the upper stratum and layers 5/6 of the lower stratum (Franco et al 2012), with layer 1 containing densely intermingled apical tufts of somata

located beneath and axons from near and far cortical neurons. Among the focal areas, M1 and ACC are classically considered an agranular areas lacking a distinct layer 4 containing non-pyramidal excitatory granular neurons (Yamawaki et al 2014).

I began with obtaining insights of differential network features juxtaposed with the divergent representations in separate functional components, by characterizing static features of neuronal population dynamics in cortical layers 1, 2, 3, and 5 (L1, L2, L3, and L5) of the four focal cortical areas SI, PPC, ACC, and MI recorded from two-photon calcium imaging in head-restrained mice (Figure 3.1, A to C). To quantify and examine spontaneous behaviors of mice, I combined videotaping (the right-side view including foretrunk, forelimb, head, and face; Figure 3.1D) and treadmill rotary records (Figure 3.2A). While the treadmill rotation captured locomotion of head-restrained mice on the setup, behavioral video also recorded non-locomotor movements which were poorly captured in treadmill rotary records, suggesting the diversity of actions during spontaneous behaviors. Accordingly, stationary (i.e. resting) and moving periods of binarily distinctive behavioral states were determined according to the motion levels quantified from the behavioral videos. To examine the comparability of data sets recorded from different cortical areas in respect to the spontaneous behavior, I analyzed individual and trial variance of spontaneous behaviors by probability distributions of movement aptitudes and moving periods (Figure 3.2B). The individual and trial variance of dynamic organizations represented in the behavioral probability distributions showed no difference among mice with different recorded cortical areas. The results provided a foundation allowing further identification of static features of neuronal population dynamics among different records.

The investigation of neuronal activities started from the simplest procedure in neuroscience: summing the activity of multiple neurons to represent a global neuronal fluctuation, and correlating this averaged activity with binary behavioral states of resting and moving (Figure 3.3A). The average activities showed highly consistent cross-area and cross-layer relations during resting and moving. Notably, average

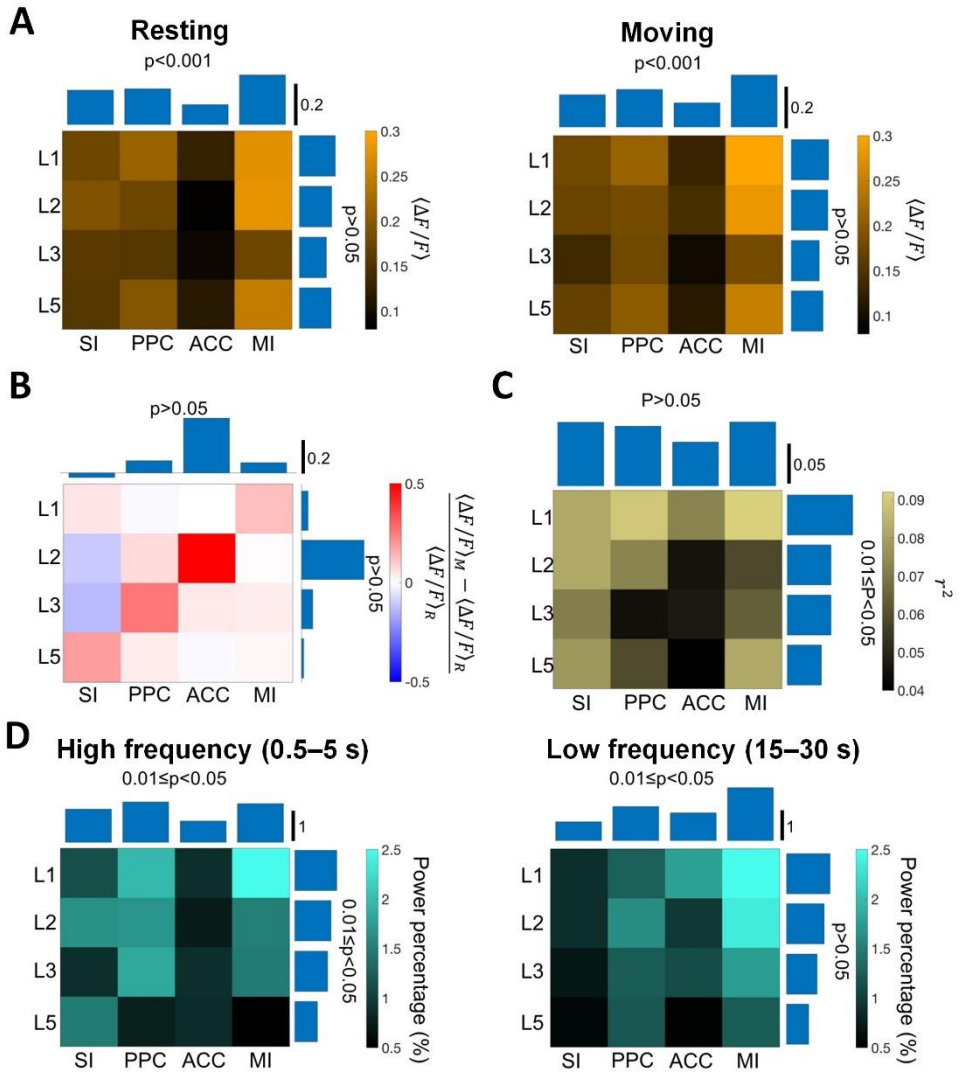

Figure 3.3. Static and dynamic features of neuronal population activity specify cortical areas and layers. **(A)** A highly consistent cross-area and cross-layer relations of the average activities between resting (left) and moving (right), with a better distinguishability across the cortical areas than along the cortical layers. **(B)** Normalized difference of average activities between resting and moving showed an area-dependent layer-specific relation. **(C)** Averaged pairwise cross-correlations of neuronal activities decreased from upper to lower cortical layer, with a less distinguishability across cortical areas. **(D)** High frequency oscillation of average activity (left) showed a similar pattern of cross-area relation than that of average activity, with a lower power percentage in layer 5. Low frequency oscillation of average activity (right) displayed both an increase along the sensorimotor axis through intracortical connections and a decrease along the axis of superficial to deep cortical layers. Mean, two-way ANOVA.

activities revealed a better distinguishability across the cortical areas than along the cortical layers. To further explore region-specified neuronal properties of behavioral function during spontaneous behaviors, I next compared the normalized difference of average activities between resting and moving (Figure 3.3B). While the normalized difference of average activities showed a poor cross-area and cross-layer distinguishability, those of SI L5, PPC L3, ACC L2, and MI L1, ordered along intracortical subnetworks, showed the highest increases for each cortical area. The result indicated that network features for identifying cortical areas and layers are both necessary to specify separate functional components in the cerebral cortex. As a second-order structure of an interacting network (Schneidman et al 2006), I observed a notable pattern that averaged pairwise cross-correlations of neuronal activities decreased from upper to lower cortical layers and showed less distinguishability across cortical areas (Figure 3.3C). To sum up, these observations so far demonstrate that the two fundamental static features of neuronal population, averaged activity and averaged pairwise cross-correlation, characterize the cortical areas and cortical layers, respectively, which further suggest a cortical map with respect to behavioral function organized by superimposing the gradients along two axes of the static features.

The difference in the static features imply the difference in the underlying network architecture and processing properties, which have a potential to regulate oscillating behaviors of self-organizing network dynamics (Engel et al 2001, Mackey & Glass 1977, Sussillo & Abbott 2009, Wang & Buzsáki 1996). To further examine potential relations between the static features and dynamic features of spontaneously ongoing neuronal activity, I investigated the power percentages of high (0.5–5 s) and low (15–30 s) frequency oscillations of average calcium activity along the cortical layers and across the cortical areas (Figure 3.3D). For the high frequent component, the cross-area relation showed a similar pattern than that of average activity, while cross-layer relation displayed a lower power percentage of high frequency oscillation in L5 of the lower cortical stratum. In contrast, power percentage of low frequency oscillation displayed both an increase along the sensorimotor axis through intracortical

connections and a decrease along the axis of superficial to deep cortical layers. Notably, power percentage of low frequency oscillation and averaged activity had different cross-area patterns, indicating a non-linear network relation between the strength of low frequency oscillation and averaged neuronal activity. Taken together, the data proposed a structural framework as a foundation for cortical operations besides neuronal representations and encoding.

3.3.2 Encoding maps of behavioral dynamics across cortical regions

Next, I investigated how neuronal representations and encoding are embedded in this structural framework of the static and dynamic features along the cortical layers across the cortical areas (Figure 3.4). To quantify the dimensionality of activity patterns embedded in a recorded neuronal population, I evaluate the percentage of the number of principle components (PCs) that captured 70% of the data variance (Figure 3.4A). Across cortical areas, while the pattern dimensionalities of neuronal populations had no significant difference between SI and PPC ($p=0.6216$; two-tailed, two-sample Student's *t* test), ACC and MI showed a higher ($p=0.0370$ compared with SI; two-tailed, two-sample Student's *t* test) and lower ($p=0.0062$ compared with SI; two-tailed, two-sample Student's *t* test) pattern dimensionality, respectively. Notably, across cortical layers, the pattern dimensionalities of neuronal populations increased with depth. Neural activity of the cerebral cortex has been known to dynamically encode behavioral state (Gentet et al 2010, Niell & Stryker 2010), which includes observations of neuronal calcium activation (Sawinski et al 2009). As expected, PCs analyzed according to temporal variance of neuronal activity showed a correlated fluctuation with the behavioral dynamics (Figure 3.4B). Over all recorded data sets in this study, the PC with the highest cross-correlation to behavioral state were primarily found among the leading PCs (Figure 3.4C). These results indicate that reafference from the dynamic of animal behavioral state was the dominant behavioral representation of cortical neuronal populations.

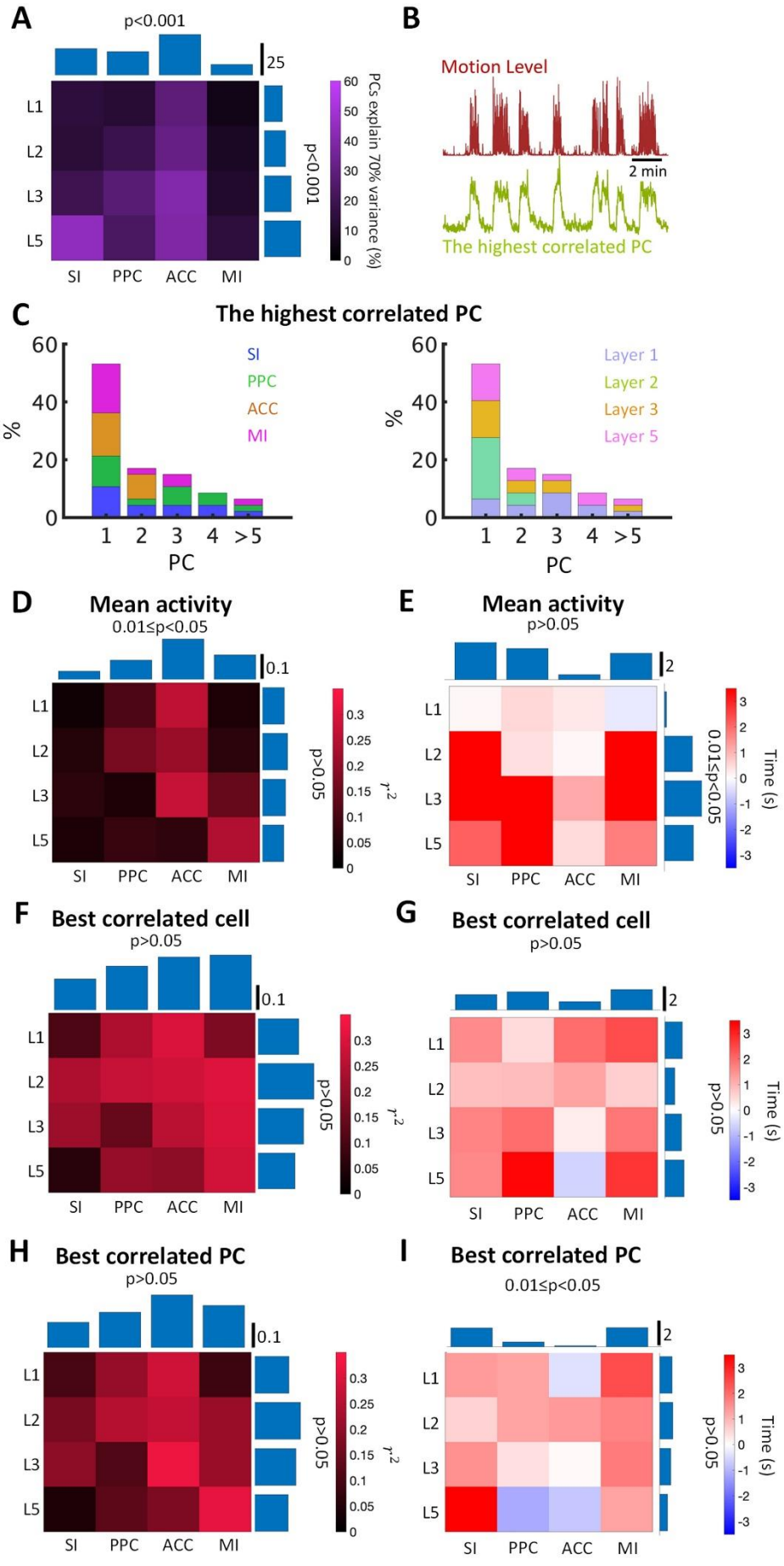
A
p<0.001
25
L1
L2
L3
L5
SI PPC ACC MI
p<0.001
PCs explain 70% variance (%)
B
Motion Level
2 min
The highest correlated PC
C
The highest correlated PC
%
SI
PPC
ACC
MI
PC
Layer 1
Layer 2
Layer 3
Layer 5
D
Mean activity
0.01≤p<0.05
0.1
p>0.05
r^2
E
Mean activity
p>0.05
2
0.01≤p<0.05
Time (s)
F
Best correlated cell
p>0.05
G
Best correlated cell
p>0.05
H
Best correlated PC
p>0.05
I
Best correlated PC
0.01≤p<0.05

Figure 3.4. Encoding map of behavioral representation in cortical neuronal populations indicates associations between neuronal and behavioral dynamics. **(A)** Pattern diversity quantified by the percentage of the number of principle components (PCs) that captured 70% of the data variance. The pattern dimensionalities of neuronal populations in deeper layers, with a higher and lower pattern dimensionality recognized in ACC and MI, respectively. **(B)** Traces of motion level and the PC with the highest cross-correlation to behavioral state emphasize a correlated fluctuation. **(C)** The highest correlated PC were mainly found among the leading PCs. **(D and E)** The strength and timing of cross-correlation between average activity and behavioral motion level. **(F and G)** Peak amplitude and timing of cross-correlation between the highest correlated neurons identified from each recorded neuronal population and behavioral motion level. **(H and I)** Peak amplitude and timing of cross-correlation between the highest correlated PC and behavioral motion level. These results imply diverse causal relationships between behavioral dynamics and multiple aspects of a single dynamical process within the same neuronal population.

To further examine cortical representations of behavioral state over the neuronal population activity in distinct cortical areas and layers, as well as their causal relationships with the behavioral dynamics, I analyzed the strength and timing of cross-correlation between neuronal activity and behavioral motion level (Figure 3.4, D to I). Average activity in ACC had a higher cross-correlation to the temporal pattern of behavioral state, while that in SI showed a lower cross-correlation (Figure 3.4D). However, the strength of cross-correlation with respect to average activity did not display a layer-specified distinguishable pattern. Moreover, a varied temporal delay of maximal correlation to the behavioral dynamics was observed in all cortical areas and layers (Figure 3.4E). The data imply that spontaneous behaviors drive a global neuronal fluctuation in the cerebral cortex.

With the consideration of divergent representations of single neurons in a neuronal population, I further investigate how this behavior-driven global fluctuation is associated with single neuron activity and how it is connected to other aspects of a single dynamical process unfolding within the same neuronal population. The cross-correlations with respect to behavioral state dynamic were compared between that of the average activity and of the highest correlated neurons identified from screening through the entire neuronal population (Figure 3.4, F and G). Behavioral representations of motion level were also observed in single neurons, which even showed a higher strength of correlation to the behavioral dynamics. In addition, beyond the consistent cross-area pattern of the cross-correlation strength as that regarding the average activity, the highest correlated neurons in L2 had higher cross-correlation strength than other layers ($p=0.0255$; two-tailed, two-sample Student's *t* test). Markedly, although a minority (4.9%; n=2 out of 41 strongest correlated neurons), a few of these strongest correlated neurons found in ACC L5 and MI L5 had their maximal correlations preceding behavioral dynamics (ranged within the bin of 81 to 243 ms). To test whether these observations imply a potential integration of these neurons with other weaker-correlated and preceding activities of single neurons, I examined the cross-correlations between behavioral motion level and the highest

correlated PCs (Figure 3.4, H and I). With a variety of correlation timing, the strength of the cross-correlations of the highest correlated PCs showed both consistent cross-area and cross-layer patterns of the cross-correlation strength as that regarding the strongest correlated neurons. Similarly, a few of these strongest correlated PCs (5.0%; n=2 out of 40 PCs) occurred in ACC L1 and L5 had a more obvious proceeding of their activity with respect to the behavioral dynamics (ranged within the bins of 1,214 to 2,185 ms). These data provide a spaciotemporal encoding map of behavioral representation in cortical neuronal populations, which further suggest a potential predictive power of neuronal activity in the cerebral cortex for future spontaneous behaviors.

3.3.3 Distinct control principles between movement maintenance and transition

To achieve implications of associations between neuronal and behavioral spontaneous dynamics, I tested their predictive powers for future states (Figure 3.5). Deterministic multiple-layer feedforward artificial neural networks (FANNs) with fixed width and depth of their network architecture were trained as predictors, which encoded a current neuronal activity at time t and decoded a future behavioral state at time $t + \tau$ (Figure 3.5, A and B), and *vice versa* (Figure 3.5C). FANN predictability was quantified by calculating the inversed value of mean squared error (MSE) compared with the data. Strikingly, by referring the first 4 leading PCs, neuronal activity was not only able to decode current behavioral motion level ($\tau = 0$ s), but also showed a predictive power for future motion level up to 10 s, the maximal time difference examined in my investigation (Figure 3.5A).

To validate the reliability of FANN prediction and compare FANN predictions by referring neuronal activity of different cortical areas and layers, I analyzed the FANN predictability along the time difference τ. Due to the integration of temporal uncertainty, predictive power of a future state should decrease with the increase of τ. This expectation matched the observation of FANN predictions (Figure 3.5B, bottom-left panel), supporting the reliability of FANN prediction. In addition, I found a

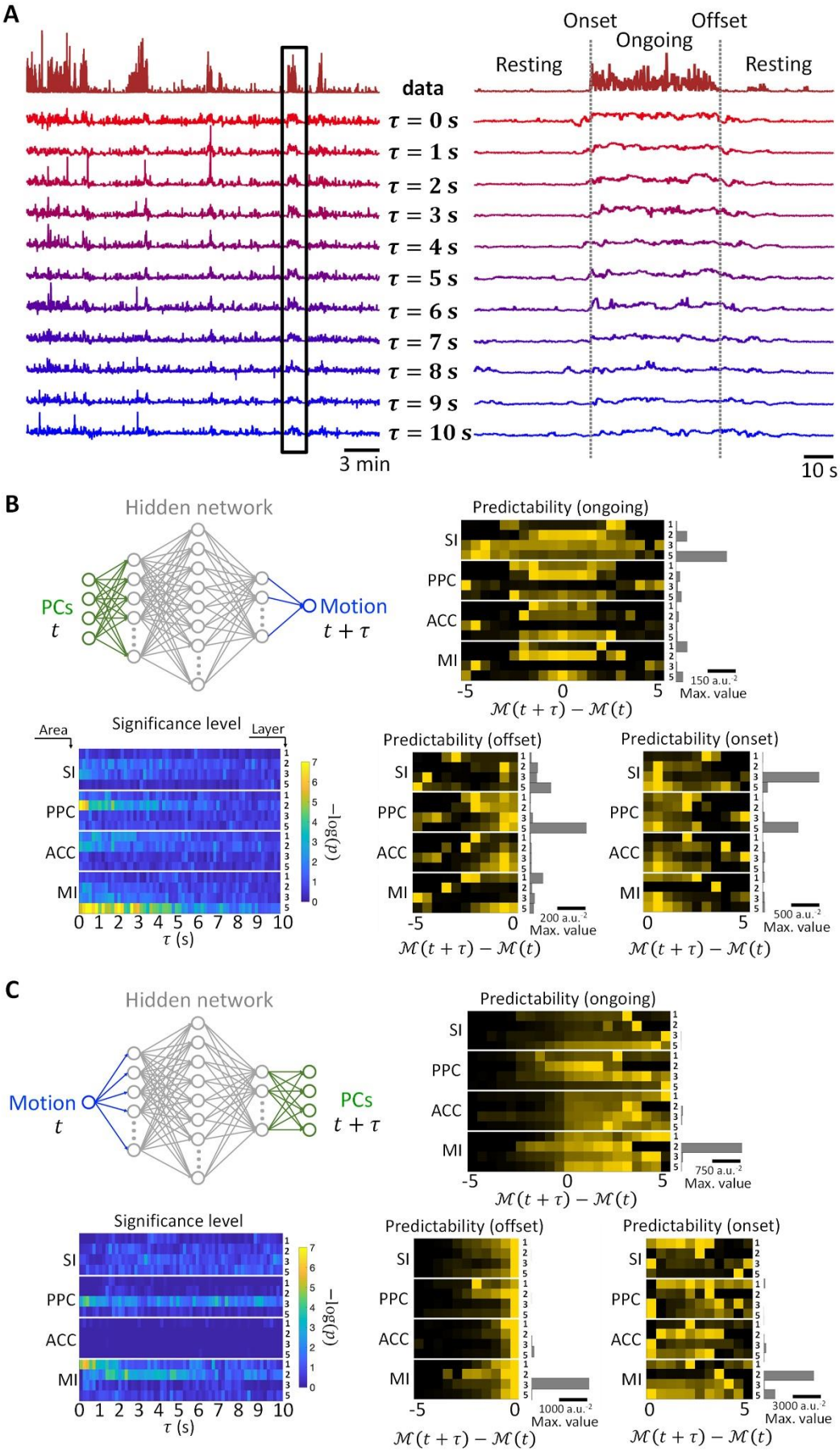
A
Onset
Offset
Ongoing
Resting
Resting
data
τ = 0 s
τ = 1 s
τ = 2 s
τ = 3 s
τ = 4 s
τ = 5 s
τ = 6 s
τ = 7 s
τ = 8 s
τ = 9 s
τ = 10 s
3 min
10 s
B
Hidden network
PCs
t
Motion
t + τ
Predictability (ongoing)
SI
PPC
ACC
MI
150 a.u.²
Max. value
M(t + τ) − M(t)
Area
Significance level
Layer
−log(p)
τ (s)
Predictability (offset)
200 a.u.²
Predictability (onset)
500 a.u.²
C
Hidden network
Motion
t
PCs
t + τ
Predictability (ongoing)
750 a.u.²
Significance level
Predictability (offset)
1000 a.u.²
Predictability (onset)
3000 a.u.²

Figure 3.5. Prediction of future behavioral and neuronal state reveals distinct control mechanisms for ongoing and transient spontaneous movements. **(A)** Neuronal activity of the first 4 leading PCs at time t predicted future motion level at time $t + \tau$. **(B)** Prediction of future motion level by neuronal activity of different cortical areas and layers. Predictability of a future state decreased when τ increase (bottom-right panel). The 3 investigations of control principles by analyzing predictability of future motion level ($\tau > 0$) with respect to the differences of motion levels in the future and present $[\mathcal{M}(t + \tau) - \mathcal{M}(t)]$ are: (i) ongoing movements (upper-right panel), with both $\mathcal{M}(t)$ and $\mathcal{M}(t + \tau)$ greater than the movement threshold, (ii) movement onset (bottom-right panel), with $\mathcal{M}(t)$ lower but $\mathcal{M}(t + \tau)$ greater than the movement threshold, and (iii) movement offset (bottom-middle panel), with $\mathcal{M}(t)$ greater but $\mathcal{M}(t + \tau)$ lower than the movement threshold. Color scale represents the inversed values of mean squared error (MSE) linearly normalized between 0 and 1, with maximal values of predictability shown in the right histograms. **(C)** Prediction of future neuronal activity of different cortical areas and layers by motion level. The results demonstrate an open-loop control for movement generation and termination (cortical activities were independent of feedback from behaviors), and a close-loop control for ongoing movement (cortical activities are dependent on feedback from behaviors).

variation of the best performance of FANN predictions by referring neuronal activity of different cortical areas and layers, with a consistent pattern across cortical areas that deeper layers presented better predictabilities for a future behavioral state. The drop of FANN predictive power were also observed when a future neuronal state was predicted by a current behavioral motion level (Figure 3.5C, bottom-left panel). While the future activities of a deeper-layer neuronal population in SI, PPC, and ACC were better predicted by behavioral motion level than those of a lower-layer neuronal population, MI showed an opposite pattern, implying an inversed reafferent influence along cortical layers in MI. The presented investigating approach and results might help to uncover control mechanisms that associate behavioral and cortical neuronal dynamics for generating, maintaining, and terminating spontaneous behaviors.

To scrutinize temporally fine-scaled control principles that connect the temporally global features shown in the dynamic organization of spontaneous neuronal activity and behaviors, I investigated association between behavioral and neuronal dynamics for generating, maintaining, and terminating spontaneous behaviors by analyzing FANN predictabilities of future neuronal and behavioral states ($\tau > 0$) with respect to the differences of motion levels between the future and present $[\mathcal{M}(t+\tau) - \mathcal{M}(t)]$ (Figure 3.5, B and C, right panels). The test of control principles for ongoing movements was focused on the FANN predictabilities with both $\mathcal{M}(t)$ and $\mathcal{M}(t+\tau)$ greater than the threshold for identifying binarily distinctive behavioral states (Figure 3.2A). For ongoing movements, neuronal activity across cortical areas and layers had their best predictabilities of future motion level when the differences of motion levels were minor [$\mathcal{M}(t+\tau) - \mathcal{M}(t)$ closed to 0] (Figure 3.5B, upper-right panel). In contrast, motion level had their best predictabilities of future neuronal activity across cortical areas and layers when motion level enhanced [$\mathcal{M}(t+\tau) - \mathcal{M}(t)$ are positive] (Figure 3.5C, upper-right panel). These results confirm, during ongoing spontaneous behaviors, a previous demonstration that the reafference from the dynamic of animal behavioral state contribute to the behavioral representation of cortical neuronal populations.

To examine whether this control principle also held for explaining the initiation and termination of spontaneous behaviors, similarly, the test of control principles for movement onsets were focused on the FANN predictabilities, but with $\mathcal{M}(t)$ lower than the threshold and $\mathcal{M}(t+\tau)$ greater than the threshold, and *vice versa* for movement offsets. For movement onsets, neuronal activity across cortical areas and layers had their best predictabilities of future motion level when the motion level slightly increased (Figure 3.5B, bottom-right panel). In contrast, motion level showed an inconsistent pattern of FANN predictabilities for future neuronal activity during movement onsets (Figure 3.5C, bottom-right panel). Moreover, for movement offsets, neuronal activity, similarly, had their best predictabilities of future motion level when the motion level slightly decreased (Figure 3.5B, bottom-middle panel), while motion level had their best predictabilities of future neuronal activity when the differences of motion levels were minor (Figure 3.5C, bottom-middle panel). Taken together, these results demonstrate that neuronal activity in the cerebral cortex lead to spontaneous movement initiation and termination, a distinct control principle for ongoing spontaneous movements.

3.4 Discussion

I present a novel approach to address previously challenging and inaccessible research problems in animal behaviors and the roles of underlying neural systems, centered on the study of the association between spontaneous behavioral and cortical neuronal dynamics in laboratory mice. These results demonstrate the first connection between temporally fine-scaled control principles and the temporally global features shown in the spontaneous neuronal and behavioral dynamics. While my data suggest a closed-loop control for ongoing movement [cortical activities are dependent on feedback from behaviors, supported by the better prediction of future neural activity from current motion level if the mice increased the motion levels during their ongoing moving (Figure 3.5C), while the prediction of future motion level from current neural activity showed wide predictability distributions with peaks when the mice displayed

weaker changes of motion levels during their ongoing moving (Figure 3.5B)] with a strong neuronal fluctuation in the cerebral cortex driven by spontaneous behaviors [e.g. a recent preprint (Stringer et al 2018)], I found little support for generalizing this control principle to explain movement initiation and termination. Instead, the data suggest an open-loop control for generating and terminating spontaneous movement [cortical activities were independent of feedback from behaviors, supported by the better prediction of future motion level from current neural activity if the mice showed a considerable increase or decrease of the motion levels during the onsets or offsets of their movement, respectively (Figure 3.5B), while the better prediction of future neural activity from current motion was only observed when the mice showed ignorable decrease during movement offset, with a rather poor prediction indicated from the disarray predictability distributions during movement onset (Figure 3.5C)]. Accordingly, I propose that organization of spontaneous behavioral dynamics is the result of collective dynamics of circuitry-wired local neuronal networks of the brain (Sussillo & Abbott 2009), while the brain-wide representation of reafference from behaviors could be taken as a strong epiphenomenon in the functional context of irregularly initiating, keeping, and suspending various behaviors for an animal in a homogenous and steady environment.

While much remains to consolidate the theory of functional framework, including a corresponding study with broader brain areas and various psychological conditions, my study provide a solid basis to uncover generalized neurobehavioral theories that explain how diverse behaviors and their controls are achieve with the brain computation. My discovery can be addressed by combining the two lines of research focuses: population-level representations in local neurons and reafference computation in neural circuits. Based on the concept that more neurons than stimulus dimensions result in freedom of representation, confusing features of divergent representations were explained as multiple aspects of a single dynamical process unfolding within the same neuronal population circuits (Mante et al 2013), which was further shown to have an advantage to maintain functional neuronal dynamics against

partial perturbation in the network (Li et al 2016). While the divergent neuronal activities were investigated for their relation to topographic arrangements, output projections, and local influence (Beyeler et al 2018, Chen et al 2013a), it remains unclear how distinct circuitry inputs are integrated in a local interacting network. Researches on another route provided a potential role of this circuitry integration, which pointed out that neuronal adjustment of reafference computation may result from a type of receptive field plasticity, called intention-dependent plasticity, involving an integration of the two receptive maps of efferent copies from the will center and of sensory inputs from the external world (Lee et al 2015). Beyond spontaneous behavior, my research approach to imply the relation between observed dynamics and underlying neuronal computation in laboratory mice opens a wide range of potentials in behavioral neuroscience.

3.5 Summary and conclusion

Despite as a well-known nature that animals outside from any behavioral task display irregular organization of spontaneous behaviors, the underlying neuronal and behavioral associations remains unclear. I approached this challenge by investigating neuronal population activities across cerebral cortical layers and areas using two-photon calcium imaging in head-restrained mice. The data characterized distinct dynamic features of neuronal population activity embedded in their region-specified static features. With the dominant representation of behavioral state, temporal encoding of behavioral dynamics varied along multiple aspects of a single population-level dynamical process. By testing predictive power for future behavioral and neuronal states, the results demonstrate an open-loop control for movement generation and termination and a close-loop control for ongoing movement. Concluding, two distinct control mechanisms of neurobehavioral association employed in producing dynamic patterns of spontaneous behaviors. My discovery in spontaneous behaviors potentially provides a fundamental and general framework for understanding the brain computations in a broader behavioral context.

4 General Discussion

4.1 Intrinsic psycho/neurobehavioral regulations in different time scales

"Man is condemned to be free; because once thrown into the world, he is responsible for everything he does." "Generally speaking there is no irreducible taste or inclination. They all represent a certain appropriative choice of being. It is up to existential psychoanalysis to compare and classify them. Ontology abandons us here; it has merely enabled us to determine the ultimate ends of human reality, its fundamental possibilities, and the value which haunts it." (Sartre 1943) Despite a rich interaction with the external cues, the two studies I presented reveal a dominant role of animal internal processes on externally expressed behaviors, either for the long-term psychobehavioral development or for the short-term spontaneous movements.

With the scope at the subcellular and single cell level, time-invariant neuronal activity is rare in the brain, not to speak of those also found a specific functional correlation (Churchland & Shenoy 2007). Divergent representations were also observed in evolutionarily ancient brain regions [e.g. neurons of the ventrolateral subdivision of ventromedial hypothalamus for aggression (Remedios et al., 2017) and medial amygdala (Li et al., 2017) in mice], indicating a generalized rule of neuronal computation embedded in these complex dynamical representations. Similarly, activity and interaction of local neuronal populations commonly fit nicely to the simulated behaviors of randomly connected recurrent networks (Mante et al 2013). However, long-range circuitry components are arranged in specific structures and connections, while their corresponding influence at the population level start to show a highly consistent and robust reactions (Li et al 2016).

Validating this knowledge, information processed in the brain is common to share similar and overlapping neural circuits (Tovote et al 2015). Such an organization even illustrates more in a massively input-converging and widespread output-projecting node that represents the source of a major neuromodulatory system, such as the dorsal

raphé nucleus as a common node for multiple serotonin functions in mouse behaviors. While it remains unknown whether the single dynamic and computational framework of neuronal population can be generalized to these brain areas that have not yet been examined, an underlying question is how the circuitry computation emerges through the associations of local neuronal networks crossing these spatial scales. An insight from the multiple-timescale recurrent neural network model applied to reveal robotic minds (Tani 2016) provides a possibility that interconnected subnetworks to which dynamics with different timescales may explain circuitry computation appearing along the spatial scale. With the presented neurophysiological support of the cross-area patterns shown in the power percentage of low and high frequency oscillation (Figure 3.3D), the long-term psychobehavioral development or short-term spontaneous movements reported in my studies can be the representations of self-organization by functional hierarchy coupled in multiple timescales. This implication emphasizes the importance of brain function for internal associations in processing information to achieve flexible and diverse performance.

4.2 Internal associations in facing the uncertain environment

"[E]ffectiveness is the specific technology of the knowledge worker within an organization. […] For manual work, we need only efficiency; that is, the ability to do things right rather than the ability to get the right things done." (Peter 1967) Animals use their single brains to face the great uncertainty in the nature and achieve countless tasks through their lives. Here I have been learning the functional role and principle, through the investigation of animal spontaneous behaviors, from such a system that has been naturally selected for its effective computational framework with an efficient circuitry organization for the challenges beyond we have imaged.

By taking system intelligence as the efficiency and effectiveness of the behaviors performed by a system in a given environment, a common feature of intelligent systems is the ability to associate their experiences with an internal representation of the external world to behave (Goodfellow et al 2016, Silver et al 2016). Comparing to

system intelligence, I propose that animals have been naturally selected more dependent on the system intelligences averaged across possible environments, called "intelligent adaptability." Based on the insights I demonstrated from the two presented studies on animal spontaneous behaviors, I argue that a common feature of system intelligent adaptability is the ability to associate diverse internal processes even in a simple task.

While the volume ratio of mammalian cerebral cortex has been increased through the evolution, with a corresponding improvement of intelligent adaptability indicated from their capability in social skills, tool usage, and artistic creation (Buckner & Krienen 2013), the cerebral cortex should play a critical role on the intelligent adaptability of a mammal. The cerebral cortex is indeed histologically and anatomically reveal a functional architecture for internal associations (Larkum 2013). My works on neuronal population dynamics of the cerebral cortex and psychobehavioral development in mice open a wide range of possibilities in academic, beyond basic research in neuroscience.

4.3 Concluding remarks

In this thesis, I firstly demonstrated a novel logical approach to identify animal emotionality in standard behavioral tests for basic research, which opens the experimental research of PTSD development during incubation period and introduce a technical advance to capture informative behavioral details. I then presented a novel investigating logic to address previously unapproachable issue in neurobehavioral dynamics for spontaneous volitional behaviors, which uncover an associative framework with two distinct control mechanisms for ongoing and transient spontaneous movements. These studies refine our basic research approach to overcome ambiguities reaching deep into the history of studies on animal spontaneous behaviors, and advance our knowledge reaching the core of neuronal computation for diverse animal behaviors.

Bibliography

Adler L, Kunz M, Chua H, Rotrosen J, Resnick S. 2004. Attention-deficit/hyperactivity disorder in adult patients with posttraumatic stress disorder (PTSD): Is ADHD a vulnerability factor? *Journal of Attention Disorders* 8: 11-16

Amadei EA, Johnson ZV, Kwon YJ, Shpiner AC, Saravanan V, et al. 2017. Dynamic corticostriatal activity biases social bonding in monogamous female prairie voles. *Nature* 546: 297-301

Anderson DJ. 2016. Circuit modules linking internal states and social behaviour in flies and mice. *Nature Reviews Neuroscience* 17: 692-704

Anderson DJ, Adolphs R. 2014. A framework for studying emotions across species. *Cell* 157: 187-200

Andrews B, Brewin CR, Philpott R, Stewart L. 2007. Delayed-onset posttraumatic stress disorder: a systematic review of the evidence. *American Journal of Psychiatry* 164: 1319-26

Angelaki DE, Cullen KE. 2008. Vestibular system: the many facets of a multimodal sense. *Annual review of neuroscience* 31: 125-50

Archer J. 1973. Tests for emotionality in rats and mice: a review. *Animal behaviour* 21: 205-35

Balogh SA, Radcliffe RA, Logue SF, Wehner JM. 2002. Contextual and cued fear conditioning in C57BL/6J and DBA/2J mice: context discrimination and the effects of retention interval. *Behavioral neuroscience* 116: 947

Banks WP, Isham EA. 2009. We infer rather than perceive the moment we decided to act. *Psychological Science* 20: 17-21

Bartal IB-A, Decety J, Mason P. 2011. Empathy and pro-social behavior in rats. *Science* 334: 1427-30

Bartal IB-A, Rodgers DA, Sarria MSB, Decety J, Mason P. 2014. Pro-social behavior in rats is modulated by social experience. *Elife* 3: e01385

Bartumeus F. 2009. Behavioral intermittence, Lévy patterns, and randomness in

animal movement. *Oikos* 118: 488-94

Bazazi S, Bartumeus F, Hale JJ, Couzin ID. 2012. Intermittent motion in desert locusts: behavioural complexity in simple environments.

Beck JS. 2011. *Cognitive behavior therapy: Basics and beyond*. Guilford Press.

Benhamou S. 2014. Of scales and stationarity in animal movements. *Ecology letters* 17: 261-72

Berkes P, Orbán G, Lengyel M, Fiser J. 2011. Spontaneous cortical activity reveals hallmarks of an optimal internal model of the environment. *Science* 331: 83-87

Berton O, McClung CA, DiLeone RJ, Krishnan V, Renthal W, et al. 2006. Essential role of BDNF in the mesolimbic dopamine pathway in social defeat stress. *Science* 311: 864-68

Beyeler A, Chang C-J, Silvestre M, Lévêque C, Namburi P, et al. 2018. Organization of valence-encoding and projection-defined neurons in the basolateral amygdala. *Cell reports* 22: 905

Boly M, Seth AK, Wilke M, Ingmundson P, Baars B, et al. 2013. Consciousness in humans and non-human animals: recent advances and future directions. *Frontiers in psychology* 4: 625

Brembs B. 2010. Towards a scientific concept of free will as a biological trait: spontaneous actions and decision-making in invertebrates. *Proceedings of the Royal Society B: Biological Sciences*: rspb20102325

Brembs B. 2011. Towards a scientific concept of free will as a biological trait: spontaneous actions and decision-making in invertebrates. *Proceedings of the Royal Society of London B: Biological Sciences* 278: 930-39

Brockmann D, Hufnagel L, Geisel T. 2006. The scaling laws of human travel. *Nature* 439: 462-65

Bryant RA, Creamer M, O'donnell M, Forbes D, McFarlane AC, et al. 2017. Acute and chronic posttraumatic stress symptoms in the emergence of posttraumatic stress disorder: a network analysis. *JAMA psychiatry* 74: 135-42

Bryant RA, O'Donnell ML, Creamer M, McFarlane AC, Silove D. 2013. A multisite

analysis of the fluctuating course of posttraumatic stress disorder. *JAMA psychiatry* 70: 839-46

Buckner RL, Krienen FM. 2013. The evolution of distributed association networks in the human brain. *Trends in cognitive sciences* 17: 648-65

Burkett JP, Andari E, Johnson ZV, Curry DC, de Waal FB, Young LJ. 2016. Oxytocin-dependent consolation behavior in rodents. *Science* 351: 375-78

Calhoon GG, Tye KM. 2015. Resolving the neural circuits of anxiety. *Nature neuroscience* 18: 1394-404

Censi A, Straw AD, Sayaman RW, Murray RM, Dickinson MH. 2013. Discriminating external and internal causes for heading changes in freely flying Drosophila. *PLoS computational biology* 9: e1002891

Chen JL, Carta S, Soldado-Magraner J, Schneider BL, Helmchen F. 2013a. Behaviour-dependent recruitment of long-range projection neurons in somatosensory cortex. *Nature* 499: 336

Chen T-W, Wardill TJ, Sun Y, Pulver SR, Renninger SL, et al. 2013b. Ultrasensitive fluorescent proteins for imaging neuronal activity. *Nature* 499: 295

Chung MC, Farmer S, Grant K, Newton R, Payne S, et al. 2003. Coping with post-traumatic stress symptoms following relationship dissolution. *Stress and Health* 19: 27-36

Churchland MM, Shenoy KV. 2007. Temporal complexity and heterogeneity of single-neuron activity in premotor and motor cortex. *Journal of neurophysiology* 97: 4235-57

Clarke R. 2002. Libertarian views: Critical survey of noncausal and event-causal accounts of free agency.

Cloninger C. 1988. Anxiety and theories of emotion. *Handbook of anxiety* 2: 1-29

Cornman JW, Lehrer K, Pappas GS. 1992. *Philosophical problems and arguments: an introduction*. Hackett Publishing.

Crawley J, Goodwin FK. 1980. Preliminary report of a simple animal behavior model for the anxiolytic effects of benzodiazepines. *Pharmacology Biochemistry and*

Behavior 13: 167-70

Cryan JF, Holmes A. 2005. The ascent of mouse: advances in modelling human depression and anxiety. *Nature reviews Drug discovery* 4: 775-90

Cullen KE. 2011. The neural encoding of self-motion. *Curr Opin Neurobiol* 21: 587-95

da Silva JA, Tecuapetla F, Paixão V, Costa RM. 2018. Dopamine neuron activity before action initiation gates and invigorates future movements. *Nature* 554: 244

Darwin C. 1872. The Expression of the Emotions in Man and Animals.

Davis M. 1989. Sensitization of the acoustic startle reflex by footshock. *Behav Neurosci* 103: 495-503

Dipoppa M, Ranson A, Krumin M, Pachitariu M, Carandini M, Harris KD. 2018. Vision and locomotion shape the interactions between neuron types in mouse visual cortex. *Neuron* 98: 602-15. e8

Driscoll LN, Pettit NL, Minderer M, Chettih SN, Harvey CD. 2017. Dynamic reorganization of neuronal activity patterns in parietal cortex. *Cell* 170: 986-99. e16

DSM-5. 2013. *Diagnostic and statistical manual of mental disorders (DSM-5®)*. American Psychiatric Association.

DSM-III. 1980. *Diagnostic and statistical manual of mental disorders (DSM-III®)*. American Psychiatric Association.

Dunn TW, Mu Y, Narayan S, Randlett O, Naumann EA, et al. 2016. Brain-wide mapping of neural activity controlling zebrafish exploratory locomotion. *Elife* 5: e12741

Ehlers A, Clark DM. 2000. A cognitive model of posttraumatic stress disorder. *Behaviour research and therapy* 38: 319-45

Engel AK, Fries P, Singer W. 2001. Dynamic predictions: oscillations and synchrony in top–down processing. *Nature Reviews Neuroscience* 2: 704

Franco SJ, Gil-Sanz C, Martinez-Garay I, Espinosa A, Harkins-Perry SR, et al. 2012. Fate-restricted neural progenitors in the mammalian cerebral cortex. *Science* 337: 746-49

Fried I, Mukamel R, Kreiman G. 2011. Internally generated preactivation of single neurons in human medial frontal cortex predicts volition. *Neuron* 69: 548-62

Funamizu A, Kuhn B, Doya K. 2016a. Neural substrate of dynamic Bayesian inference in the cerebral cortex. *Nature neuroscience*

Funamizu A, Kuhn B, Doya K. 2016b. Neural substrate of dynamic Bayesian inference in the cerebral cortex. *Nature neuroscience* 19: 1682

Gentet LJ, Avermann M, Matyas F, Staiger JF, Petersen CC. 2010. Membrane potential dynamics of GABAergic neurons in the barrel cortex of behaving mice. *Neuron* 65: 422-35

Golden SA, Covington III HE, Berton O, Russo SJ. 2011. A standardized protocol for repeated social defeat stress in mice. *Nature protocols* 6: 1183-91

Goodfellow I, Bengio Y, Courville A, Bengio Y. 2016. *Deep learning*. MIT press Cambridge.

Goto T, Kubota Y, Tanaka Y, Iio W, Moriya N, Toyoda A. 2014. Subchronic and mild social defeat stress accelerates food intake and body weight gain with polydipsia-like features in mice. *Behavioural brain research* 270: 339-48

Grupe DW, Nitschke JB. 2013. Uncertainty and anticipation in anxiety: an integrated neurobiological and psychological perspective. *Nature Reviews Neuroscience* 14: 488-501

Haggard P. 2008. Human volition: towards a neuroscience of will. *Nature Reviews Neuroscience* 9: 934-46

Haggard P, Eimer M. 1999. On the relation between brain potentials and the awareness of voluntary movements. *Experimental Brain Research* 126: 128-33

Halko N, Martinsson P-G, Tropp JA. 2011. Finding structure with randomness: Probabilistic algorithms for constructing approximate matrix decompositions. *SIAM review* 53: 217-88

Hall C, Ballachey EL. 1932. A study of the rat's behavior in a field. A contribution to method in comparative psychology. *University of California Publications in Psychology*

Hashikawa K, Hashikawa Y, Tremblay R, Zhang J, Feng JE, et al. 2017. Esr1+ cells in the ventromedial hypothalamus control female aggression. *Nature neuroscience* 20: 1580

Hayes JP, VanElzakker MB, Shin LM. 2012. Emotion and cognition interactions in PTSD: a review of neurocognitive and neuroimaging studies. *Frontiers in integrative neuroscience* 6

Hetrick SE, Purcell R, Garner B, Parslow R. 2010. Combined pharmacotherapy and psychological therapies for post traumatic stress disorder (PTSD). *The Cochrane Library*

Hoopfer ED, Jung Y, Inagaki HK, Rubin GM, Anderson DJ. 2015. P1 interneurons promote a persistent internal state that enhances inter-male aggression in Drosophila. *Elife* 4: e11346

Jin X, Costa RM. 2010. Start/stop signals emerge in nigrostriatal circuits during sequence learning. *Nature* 466: 457

Kafetzopoulos E, Gouskos S, Evangelou SN. 1997. 1/f Noise and multifractal fluctuations in rat behavior. *Nonlinear Analysis* 30: 2007-13

Kagaya K, Takahata M. 2011. Sequential synaptic excitation and inhibition shape readiness discharge for voluntary behavior. *Science* 332: 365-68

Kaouane N, Porte Y, Vallée M, Brayda-Bruno L, Mons N, et al. 2012. Glucocorticoids can induce PTSD-like memory impairments in mice. *Science* 335: 1510-13

Kato S, Kaplan HS, Schrödel T, Skora S, Lindsay TH, et al. 2015. Global brain dynamics embed the motor command sequence of Caenorhabditis elegans. *Cell* 163: 656-69

Kawai R, Markman T, Poddar R, Ko R, Fantana AL, et al. 2015. Motor cortex is required for learning but not for executing a motor skill. *Neuron* 86: 800-12

Ko J. 2017. Neuroanatomical Substrates of Rodent Social Behavior: The Medial Prefrontal Cortex and Its Projection Patterns. *Frontiers in Neural Circuits* 11: 41

Krishnan V, Han M-H, Graham DL, Berton O, Renthal W, et al. 2007. Molecular adaptations underlying susceptibility and resistance to social defeat in brain

reward regions. *Cell* 131: 391-404

Kühn S, Brass M. 2009. Retrospective construction of the judgement of free choice. *Consciousness and cognition* 18: 12-21

Kumar V, Bhat ZA, Kumar D. 2013. Animal models of anxiety: a comprehensive review. *Journal of pharmacological and toxicological methods* 68: 175-83

Larkum M. 2013. A cellular mechanism for cortical associations: an organizing principle for the cerebral cortex. *Trends in neurosciences* 36: 141-51

Lau HC, Rogers RD, Haggard P, Passingham RE. 2004. Attention to intention. *science* 303: 1208-10

Lau HC, Rogers RD, Passingham RE. 2007. Manipulating the experienced onset of intention after action execution. *Journal of cognitive neuroscience* 19: 81-90

Lee RX, Huang J-J, Huang C, Tsai M-L, Yen C-T. 2015. Plasticity of cerebellar Purkinje cells in behavioral training of body balance control. *Frontiers in systems neuroscience* 9: 113

Lee RX, Huang JJ, Huang C, Tsai ML, Yen CT. 2014. Collateral projections from vestibular nuclear and inferior olivary neurons to lobules I/II and IX/X of the rat cerebellar vermis: a double retrograde labeling study. *European Journal of Neuroscience* 40: 2811-21

Lee RX, Stephens GJ, Kuhn B. 2018. Affective bonding explains post-traumatic behavioral development in adult mice. *bioRxiv*: 249870

Li N, Daie K, Svoboda K, Druckmann S. 2016. Robust neuronal dynamics in premotor cortex during motor planning. *Nature* 532: 459

Libet B. 2003. Can conscious experience affect brain activity? *Journal of Consciousness Studies* 10: 24-28

Libet B, Gleason CA, Wright EW, Pearl DK. 1983. Time of conscious intention to act in relation to onset of cerebral activity (readiness-potential) the unconscious initiation of a freely voluntary act. *Brain* 106: 623-42

Lin D, Boyle MP, Dollar P, Lee H, Lein E, et al. 2011. Functional identification of an aggression locus in the mouse hypothalamus. *Nature* 470: 221

Low RJ, Gu Y, Tank DW. 2014. Cellular resolution optical access to brain regions in fissures: imaging medial prefrontal cortex and grid cells in entorhinal cortex. *Proceedings of the National Academy of Sciences* 111: 18739-44

Luczak A, Barthó P, Harris KD. 2009. Spontaneous events outline the realm of possible sensory responses in neocortical populations. *Neuron* 62: 413-25

Mackey MC, Glass L. 1977. Oscillation and chaos in physiological control systems. *Science* 197: 287-89

Mante V, Sussillo D, Shenoy KV, Newsome WT. 2013. Context-dependent computation by recurrent dynamics in prefrontal cortex. *nature* 503: 78

Mataix-Cols D, de la Cruz LF, Monzani B, Rosenfield D, Andersson E, et al. 2017. D-Cycloserine Augmentation of Exposure-Based Cognitive Behavior Therapy for Anxiety, Obsessive-Compulsive, and Posttraumatic Stress Disorders: A Systematic Review and Meta-analysis of Individual Participant Data. *JAMA psychiatry* 74: 501-10

Matsuhashi M, Hallett M. 2008. The timing of the conscious intention to move. *European Journal of Neuroscience* 28: 2344-51

Maye A, Hsieh C-h, Sugihara G, Brembs B. 2007. Order in spontaneous behavior. *PloS one* 2: e443

McFarlane AC. 2010. The long-term costs of traumatic stress: intertwined physical and psychological consequences. *World Psychiatry* 9: 3-10

McHugh PR, Treisman G. 2007. PTSD: A problematic diagnostic category. *Journal of anxiety disorders* 21: 211-22

Miczek KA, O'Donnell JM. 1978. Intruder-evoked aggression in isolated and nonisolated mice: effects of psychomotor stimulants and L-dopa. *Psychopharmacology* 57: 47-55

Monson CM, Fredman SJ, Macdonald A, Pukay-Martin ND, Resick PA, Schnurr PP. 2012. Effect of cognitive-behavioral couple therapy for PTSD: A randomized controlled trial. *JAMA* 308: 700-09

Mostoufi S, Godfrey KM, Ahumada SM, Hossain N, Song T, et al. 2014. Pain sensitivity

in posttraumatic stress disorder and other anxiety disorders: a preliminary case control study. *Annals of general psychiatry* 13: 31

Müller CA, Schmitt K, Barber AL, Huber L. 2015. Dogs can discriminate emotional expressions of human faces. *Current Biology* 25: 601-05

Murakami M, Vicente MI, Costa GM, Mainen ZF. 2014. Neural antecedents of self-initiated actions in secondary motor cortex. *Nature neuroscience*

Nagel T. 1974. What is it like to be a bat? *The philosophical review* 83: 435-50

Nakamura T, Kiyono K, Yoshiuchi K, Nakahara R, Struzik ZR, Yamamoto Y. 2007. Universal scaling law in human behavioral organization. *Physical review letters* 99: 138103

Nakamura T, Takumi T, Takano A, Aoyagi N, Yoshiuchi K, et al. 2008. Of mice and men—universality and breakdown of behavioral organization. *PLoS One* 3: e2050

Niell CM, Stryker MP. 2010. Modulation of visual responses by behavioral state in mouse visual cortex. *Neuron* 65: 472-79

Oizumi M, Albantakis L, Tononi G. 2014. From the phenomenology to the mechanisms of consciousness: integrated information theory 3.0. *PLoS computational biology* 10: e1003588

Oizumi M, Tsuchiya N, Amari S-i. 2016. Unified framework for information integration based on information geometry. *Proceedings of the National Academy of Sciences* 113: 14817-22

Otabi H, Goto T, Okayama T, Kohari D, Toyoda A. 2017. The acute social defeat stress and nest-building test paradigm: A potential new method to screen drugs for depressive-like symptoms. *Behavioural Processes* 135: 71-75

Pai A, Suris AM, North CS. 2017. Posttraumatic Stress Disorder in the DSM-5: Controversy, Change, and Conceptual Considerations. *Behavioral Sciences* 7: 7

Pamplona F, Henes K, Micale V, Mauch C, Takahashi R, Wotjak C. 2011. Prolonged fear incubation leads to generalized avoidance behavior in mice. *Journal of psychiatric research* 45: 354-60

Parga N, Abbott LF. 2007. Network model of spontaneous activity exhibiting synchronous transitions between up and down states. *Frontiers in Neuroscience* 1: 4

Patki G, Solanki N, Salim S. 2014. Witnessing traumatic events causes severe behavioral impairments in rats. *International Journal of Neuropsychopharmacology* 17: 2017-29

Pellow S, Chopin P, File SE, Briley M. 1985. Validation of open: closed arm entries in an elevated plus-maze as a measure of anxiety in the rat. *Journal of neuroscience methods* 14: 149-67

Peron SP, Freeman J, Iyer V, Guo C, Svoboda K. 2015. A cellular resolution map of barrel cortex activity during tactile behavior. *Neuron* 86: 783-99

Peter FD. 1967. The effective executive. *New York, Harper&Row*

Pfeiffer BE, Foster DJ. 2013. Hippocampal place-cell sequences depict future paths to remembered goals. *Nature* 497: 74-79

Philbert J, Pichat P, Beeske S, Decobert M, Belzung C, Griebel G. 2011. Acute inescapable stress exposure induces long-term sleep disturbances and avoidance behavior: a mouse model of post-traumatic stress disorder (PTSD). *Behavioural brain research* 221: 149-54

Proekt A, Banavar JR, Maritan A, Pfaff DW. 2012. Scale invariance in the dynamics of spontaneous behavior. *Proceedings of the National Academy of Sciences* 109: 10564-69

Ramos-Fernández G, Mateos JL, Miramontes O, Cocho G, Larralde H, Ayala-Orozco B. 2004. Lévy walk patterns in the foraging movements of spider monkeys (Ateles geoffroyi). *Behavioral Ecology and Sociobiology* 55: 223-30

Ramos A. 2008. Animal models of anxiety: do I need multiple tests? *Trends in pharmacological sciences* 29: 493-98

Remedios R, Kennedy A, Zelikowsky M, Grewe BF, Schnitzer MJ, Anderson DJ. 2017. Social behaviour shapes hypothalamic neural ensemble representations of conspecific sex. *Nature* 550: 388

Reynolds AM, Frye MA. 2007. Free-flight odor tracking in Drosophila is consistent with an optimal intermittent scale-free search. *PloS one* 2: e354

Rochefort C, Lefort JM, Rondi-Reig L. 2013. The cerebellum: a new key structure in the navigation system. *Front Neural Circuits* 7: 35

Rolls E, Deco G. 2011. Prediction of decisions from noise in the brain before the evidence is provided. *Decision Neuroscience* 5: 33

Roome CJ, Kuhn B. 2014. Chronic cranial window with access port for repeated cellular manipulations, drug application, and electrophysiology. *Frontiers in cellular neuroscience* 8: 379

Rosner R, Warzecha A-K. 2011. Relating neuronal to behavioral performance: variability of optomotor responses in the blowfly. *PLoS One* 6: e26886

Sandi C, Haller J. 2015. Stress and the social brain: behavioural effects and neurobiological mechanisms. *Nature Reviews Neuroscience* 16: 290-304

Sapolsky RM. 2002. Chickens, eggs and hippocampal atrophy. *Nature neuroscience* 5: 1111-14

Sartre J-P. 1943. *Being and nothingness*. Open Road Media.

Sawinski J, Wallace DJ, Greenberg DS, Grossmann S, Denk W, Kerr JN. 2009. Visually evoked activity in cortical cells imaged in freely moving animals. *Proceedings of the National Academy of Sciences* 106: 19557-62

Schneidman E, Berry II MJ, Segev R, Bialek W. 2006. Weak pairwise correlations imply strongly correlated network states in a neural population. *Nature* 440: 1007

Schnyder U, Cloitre M. 2015. *Evidence based treatments for trauma-related psychological disorders: A practical guide for clinicians*. Springer.

Sial OK, Warren BL, Alcantara LF, Parise EM, Bolaños-Guzmán CA. 2016. Vicarious social defeat stress: Bridging the gap between physical and emotional stress. *Journal of neuroscience methods* 258: 94-103

Siegmund A, Wotjak CT. 2006. Toward an animal model of posttraumatic stress disorder. *Annals of the New York Academy of Sciences* 1071: 324-34

Silver D, Huang A, Maddison CJ, Guez A, Sifre L, et al. 2016. Mastering the game of

Go with deep neural networks and tree search. *nature* 529: 484

Smith ML, Hostetler CM, Heinricher MM, Ryabinin AE. 2016. Social transfer of pain in mice. *Science advances* 2: e1600855

Song C, Koren T, Wang P, Barabási A-L. 2010. Modelling the scaling properties of human mobility. *Nature Physics* 6: 818-23

Stephens GJ, de Mesquita MB, Ryu WS, Bialek W. 2011a. Emergence of long timescales and stereotyped behaviors in Caenorhabditis elegans. *Proceedings of the National Academy of Sciences* 108: 7286-89

Stephens GJ, Johnson-Kerner B, Bialek W, Ryu WS. 2008. Dimensionality and dynamics in the behavior of C. elegans. *PLoS computational biology* 4: e1000028

Stephens GJ, Osborne LC, Bialek W. 2011b. Searching for simplicity in the analysis of neurons and behavior. *Proceedings of the National Academy of Sciences* 108: 15565-71

Sterley T-L, Baimoukhametova D, Füzesi T, Zurek AA, Daviu N, et al. 2018. Social transmission and buffering of synaptic changes after stress. *Nature neuroscience* 21: 393

Stringer C, Pachitariu M, Steinmetz N, Reddy CB, Carandini M, Harris KD. 2018. Spontaneous behaviors drive multidimensional, brain-wide population activity. *bioRxiv*: 306019

Stringer C, Pachitariu M, Steinmetz NA, Okun M, Bartho P, et al. 2016. Inhibitory control of correlated intrinsic variability in cortical networks. *Elife* 5: e19695

Sussillo D, Abbott LF. 2009. Generating coherent patterns of activity from chaotic neural networks. *Neuron* 63: 544-57

Takahashi A, Lee RX, Iwasato T, Itohara S, Arima H, et al. 2015. Glutamate input in the dorsal raphe nucleus as a determinant of escalated aggression in male mice. *Journal of Neuroscience* 35: 6452-63

Tani J. 2016. *Exploring robotic minds: actions, symbols, and consciousness as self-organizing dynamic phenomena*. Oxford University Press.

Tononi G. 2004. An information integration theory of consciousness. *BMC neuroscience*

5: 42

Tononi G, Boly M, Massimini M, Koch C. 2016. Integrated information theory: from consciousness to its physical substrate. *Nature Reviews Neuroscience* 17: 450

Tovote P, Fadok JP, Lüthi A. 2015. Neuronal circuits for fear and anxiety. *Nature Reviews Neuroscience* 16: 317

Trevena J, Miller J. 2010. Brain preparation before a voluntary action: Evidence against unconscious movement initiation. *Consciousness and cognition* 19: 447-56

Tsuda MC, Yeung H-M, Kuo J, Usdin TB. 2015. Incubation of fear is regulated by TIP39 peptide signaling in the medial nucleus of the amygdala. *Journal of Neuroscience* 35: 12152-61

Velmans M. 2003. Preconscious free will. *Journal of Consciousness Studies* 10: 42-61

Walton JL, Cuccurullo LAJ, Raines AM, Vidaurri DN, Allan NP, et al. 2017. Sometimes Less is More: Establishing the Core Symptoms of PTSD. *Journal of Traumatic Stress*

Wang X-J, Buzsáki G. 1996. Gamma oscillation by synaptic inhibition in a hippocampal interneuronal network model. *Journal of neuroscience* 16: 6402-13

Warren BL, Vialou VF, Iñiguez SD, Alcantara LF, Wright KN, et al. 2013. Neurobiological sequelae of witnessing stressful events in adult mice. *Biological psychiatry* 73: 7-14

Yadav CK, Verma MK, Ghosh S. 2010. Statistical evidence for power law temporal correlations in exploratory behaviour of rats. *BioSystems* 102: 77-81

Yamawaki N, Borges K, Suter BA, Harris KD, Shepherd GM. 2014. A genuine layer 4 in motor cortex with prototypical synaptic circuit connectivity. *Elife* 3: e05422

Yoo J-C, Han TH. 2009. Fast normalized cross-correlation. *Circuits, systems and signal processing* 28: 819

Zingg B, Hintiryan H, Gou L, Song MY, Bay M, et al. 2014. Neural networks of the mouse neocortex. *Cell* 156: 1096-111

Zoladz PR, Diamond DM. 2013. Current status on behavioral and biological markers of PTSD: a search for clarity in a conflicting literature. *Neuroscience & Biobehavioral Reviews* 37: 860-95